THE PENNSYLVANIA STATE UNIVERSITY
SCHREYER HONORS COLLEGE

DEPARTMENT OF ELECTRICAL ENGINEERING

DESIGN OF A ROCKET-BORNE IN SITU PLASMA FREQUENCY PROBE

BRIAN C. SCHRATZ

Spring 2006

A thesis
submitted in partial fulfillment
of the requirements
for a baccalaureate degree
in Electrical Engineering
with honors in Electrical Engineering

Reviewed and approved* by the following:

Dr. Sven G. Bilén
Associate Professor of Engineering Design and Electrical Engineering
Thesis Supervisor and Honors Advisor

Dr. John D. Mitchell
Professor of Electrical Engineering
Faculty Reader

Dr. C. Russell Philbrick
Professor of Electrical Engineering
Faculty Reader

Dr. W. Kenneth Jenkins
Department Head of Electrical Engineering

* Signatures on file in the Schreyer Honors College.

We approve the thesis of Brian C. Schratz:

Date of Signature

Dr. Sven G. Bilén Associate Professor of Engineering Design and Electrical Engineering Thesis Supervisor and Honors Advisor	
Dr. John D. Mitchell Professor of Electrical Engineering Faculty Reader	
Dr. C. Russell Philbrick Professor of Electrical Engineering Faculty Reader	
Dr. W. Kenneth Jenkins Department Head of Electrical Engineering	

9-4188-5313

ABSTRACT

This work explores the design of a digitally controlled Plasma Frequency Probe (PFP) instrument. Flight tests aboard a NASA sounding rocket (Terrier Improved-Orion 41.056) will demonstrate the validity of the complete instrument to measure atmospheric plasma frequency between altitudes of 60 to 180 km. Plasma frequency represents the settling time of the plasma to an externally applied field that the probe will radiate. The probe identifies the resonance frequency of the plasma by sweeping through a range of frequencies and recording the frequency at which the return signal exhibits a zero-phase difference and a maximum magnitude compared to the radiated signal. This represents the plasma resonance. Furthermore, as electrons collide with neutral particles, the quality factor of the resonance peak will degrade. Using these measurements and other known constants, the instrument can make a direct measure of plasma density as well as determine the ion collision frequency. Atmospheric and space science has been and continues to be an important topic of research within Penn State's Department of Electrical Engineering. The investigation of atmospheric dynamics is relevant to our understanding of the propagation of radio waves in the atmosphere, the connection between the sun and our planet, and space weather.

TABLE OF CONTENTS

LIST OF FIGURES

ACKNOWLEDGEMENTS

I could not have completed this project without a team of incredible individuals. My sincere thanks go to all of those people who helped me over these past years. I would like to especially thank my advisor and mentor, Dr. Sven Bilén for his continued advice, support, and encouragement. He has given me opportunities that exceeded my wildest dreams.

Dr. Russell Philbrick has generously lent his continued support and his incredible experience to advance my efforts in this project. His demonstrated interest in the Plasma Frequency Probe (PFP) and the entire SPIRIT III project has been vital to its successes.

Robert Siegel's previous work on earlier versions of the PFP and LionSat's Hybrid Plasma Probe served as a foundation for this project and I would like to thank him for his continued involvement, friendship, and advice.

The credit for the structural work goes completely to my fellow students, Jon Cumblad and Ed Brouwers. Their combined assistance with the structural components of this experiment, their expert skill in design and fabrication, and their unending patience with my many changes has been an invaluable contribution.

My fellow students Andrew Cooney, Mike Fenton, Matthew Sunderland, and Erik Weir were instrumental in the fabrication, assembly, and testing of this design. Working with you all has been a pleasure; I could not have finished this without your assistance.

My many thanks go out to Dr. John Mitchell and Professor Wharton, for their many consults on a wide range of topics.

I could not have created the PFP without the Pennsylvania Space Grant Consortium's generous sponsorship of the SPIRIT sounding rocket project. The Consortium's support has positively affected my life and the lives of countless other students over the years.

And finally, I give my most heart-felt thanks and absolute gratitude to my parents, Dr. and Mrs. Paul and Patricia Schratz. Your many years of support, sacrifice, encouragement, and advice are the reason I have accomplished all that I have. Your examples taught me the value of education and of hard work. You have inspired me with the motivation and drive required for achieving all that I have. Know that as I reach for the stars, I am standing on your shoulders.

Chapter 1

Science and Motivation

1.1 Background

Plasma is a collection of charged particles where the net charge is approximately neutral on a macroscopic scale, although localized charged regions may exists. In earth's atmosphere, plasma is the result of radiation from the sun ionizing gases in the atmosphere. During the night, plasma density in the atmosphere decreases due to recombination. But recombination is too slow for the plasma to dissipate altogether.

Plasma also varies with altitude as the concentration and species of gas molecules varies with altitudes. Figure **1-1** shows plasma density as a function of altitude and time of day.

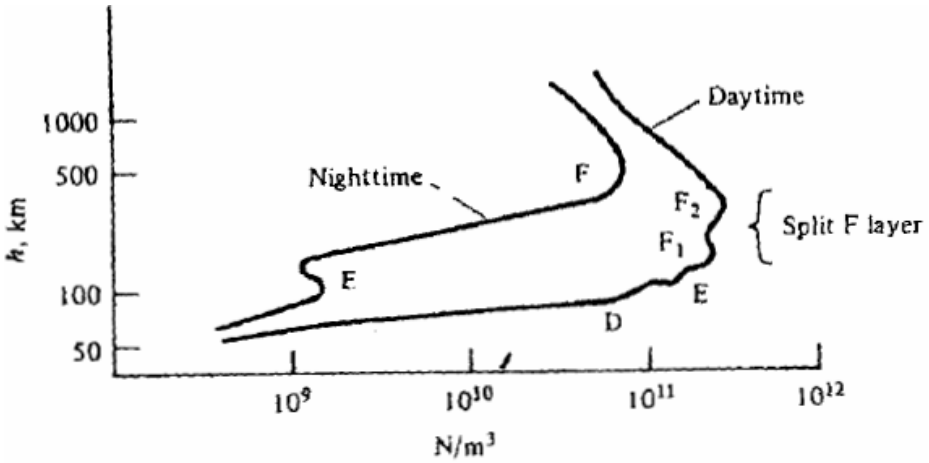

Figure **1-1**: Plasma Density Versus Altitude
(source: Collin 389)

Atmospheric plasma consists of electrons and positive ions. If an external source perturbs the plasma, it will repulse this force. Since electrons are much smaller than the ions, they possessive higher velocities than the heavier ions and so respond faster to an external source. When this force is removed, the plasma will compensate for the charge imbalance using coulomb forces—the electrons will return to their original location but because of momentum, they will overshoot and oscillate around the positive ion. This oscillation mimics that of a simple mechanical spring model. The rate of oscillation, or plasma frequency, is directly dependent on the density of the plasma. Both positive ions and electrons oscillate, but because of the difference in velocities of the particles (due to respective size), electrons dominate the plasma oscillation.

To illustrate this process, consider two uniformly charged sheets; one with negatively charged electrons and one with positively charged ions. Figure **1-2** illustrates these sheets with the negatively charged sheet displaced by some distance, Δx. Region 1

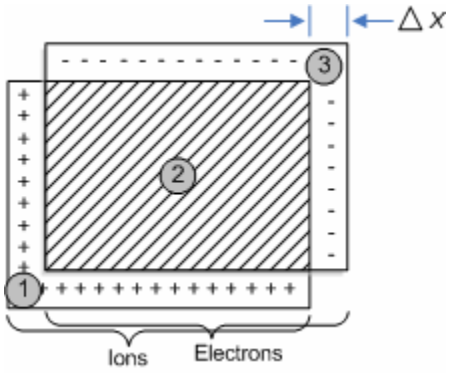

Figure **1-2**: Type Caption Here

is the sheet of positive charge, region 3 is the sheet of negative charge, and region 2 is where regions 1 and 3 overlap. The electric field will develop because of the displacements and its vector points from the positive sheet towards the negative sheet. The electric field outside these three regions is zero.

This separation Δx causes an electric field to develop between the two plates that can be solved for using Gauss' law, $\varepsilon_0 \oint \vec{E} \bullet d\vec{A} = q_{enclosed}$. The term $\oint \vec{E} \bullet d\vec{A}$ represents the electric flux through the Gaussian surface. In this simple case, $\vec{E}A$ replaces the electric flux integral. The enclosed charge is simply the charge per unit area, σ, multiplied with the area, A. The charge density that develops between the slabs due to the displacement is $(en_0\Delta x)$ where e is the electron charge and n_0 is the number of electrons per unit volume. Substituting these simplifications into Gauss' law yields a solution for the electric field.

$$\vec{E} = \frac{n_0 e \Delta \vec{x}}{\varepsilon_0} \qquad \textbf{1.1}$$

When an external force displaces these electrons, the induced electric field exerts a force, $-e\vec{E}$, on the particles. The equation of motion for this force is simply Newton's second law, *force* = *mass* x *acceleration*, or

$$F = m_e \frac{d^2 \Delta x}{dt^2} \qquad \textbf{1.2}$$

Combining Eq. **1.1** and Eq. **1.2** and rearranging yields a second order homogeneous differential equation. Eq. **1.3**

$$\frac{d^2 \Delta x}{dt^2} + \left(\frac{n_0 e^2}{\varepsilon_0 m_e} \right) \Delta x = 0 \qquad \textbf{1.3}$$

This result is the equation for a harmonic oscillator with the frequency of oscillation determined by the term in parenthesis. The frequency is

$$\omega_{pe}^2 = \frac{n_0 e^2}{\varepsilon_0 m_e} \qquad \textbf{1.4}$$

Eq. **1.4** assumes that there are no collisions between electrons and ions. The addition of collision effects adds a damping factor $-\nu m_e \frac{d\Delta x}{dt}$ in Eq. **1.3** where ν is the collision frequency. Collision frequency becomes increasingly dominant in lower altitudes as the concentration of molecules is higher. Section **1.2** illustrates the effects of this additional term while explaining an application of plasma frequency.

In addition to collision frequency, the measured plasma frequency will have one other additional contribution: the Earth's magnetic field. The Lorenz Force describes the force of an electron in an electric field as

$$\vec{F} = -e\left(\vec{E} + \vec{v}_e \times \vec{B}\right) = m_e \frac{d\vec{v}_e}{dt} \qquad \textbf{1.5}$$

where $\vec{v}_e$ is the electron velocity (different from collision frequency ν addressed previously) through a uniform magnetic field $\vec{B}$. In the absence of an electric field $\vec{E}$ and a magnetic field perpendicular to the electron velocity, the electron will enter a circular orbit with angular frequency

$$\omega_{ce} = \frac{eB}{m_e} \qquad \textbf{1.6}$$

called the cyclotron frequency. Eq. **1.6** does not account for the force on the electron applied by the electric field. This addition represents drift in the electron trajectory and translates to electrons traveling along the Earth's magnetic field lines.

The contributions of the electron plasma frequency assuming no drift and magnetic effects and the electron cyclotron frequency combine to form an upper hybrid frequency ω_{uh} shown in equation **1.7**.

$$\omega_{uh} = \sqrt{\omega_{pe} + \omega_{ce}} \qquad \textbf{1.7}$$

Figure **Figure 1.3** shows illustrates the range of frequencies for plasma frequency, collision frequency, and cyclotron frequency as a function of altitude. Notice how collision frequency decreases with altitude as the density of the atmosphere decreases. Also notice how the plasma frequency peaks sharply around 85 km and then dips slightly around 120 km. This is consistent with the peaks and drops in plasma density shown in Figure **1-1**. The cyclotron frequency (also referred to as the gyro frequency) remains roughly constant.

All derivations in previous examples have examined the behavior of electrons in the plasma environment. Heavier molecule ions also have the same equations of motion as electrons. However, as this section mentions above, the small relative size of electrons compared to heavier ions makes the electrons the dominant contribution to these frequency calculations. To include the effects of all species in the plasma, similar derivations exist as the ones presented here.

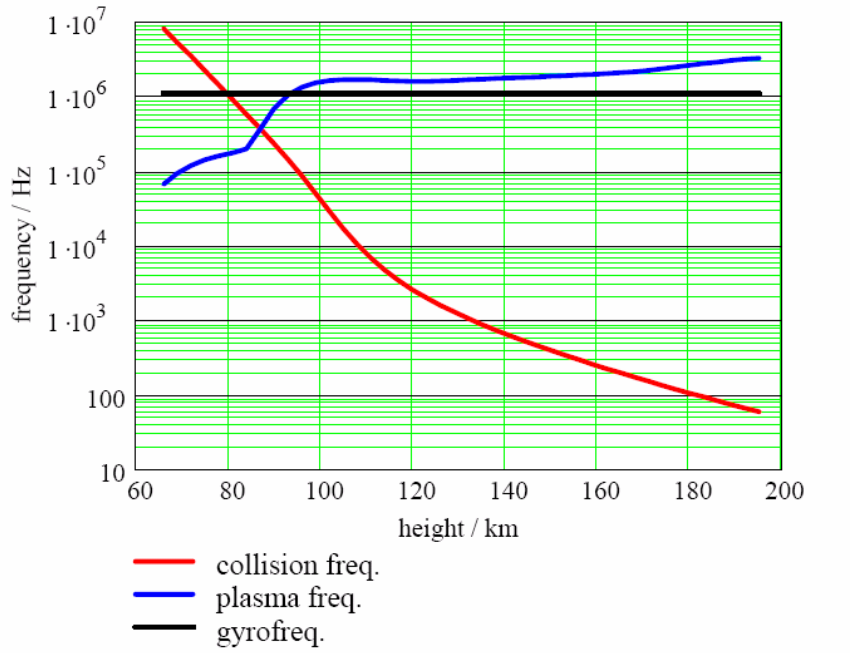

Figure **1.3**: Plasma Frequency Contributions Versus Altitude

Figure out when SPIRIT goes flat spin. Compare to i-scat ground based measurements—use this as a way to adjust the range of the frequency sweep right before launch.

1.2 Effects on Radio Wave Reflection

Common radio communications achieve ranges beyond the horizon (farther than simple line-of-sight allows) by using the Earth's ionosphere to reflect radio waves. The characteristics of ionospheric reflection depend directly on plasma frequency. To illustrate the dependence of plasma frequency, one begins with examining a single electron in an electric field. The force on this electron is equal to both the electron charge, -*e*, multiplied by the applied electric field, $\vec{E}$, and the electron mass, m_e, multiplied by the particle's acceleration $d\vec{v}/dt$.

$$\vec{F} = -e\vec{E} = m_e \frac{d\vec{v}}{dt} \qquad \textbf{1.8}$$

Eq. **1.9** and Eq. **1.10** show the phasor representation for the time varying electric field and velocity vectors. Eq. **1.9** and Eq. **1.10** can be substituted into Eq. **1.8** to replace the electric field and velocity vectors. Taking the derivative of the velocity vector and solving for velocity yields Eq. **1.11**.

$$\vec{E} = \mathrm{Re}\{\vec{E}e^{j\omega t}\} \qquad \textbf{1.9}$$

$$\vec{v} = \mathrm{Re}\{\vec{V}e^{j\omega t}\} \qquad \textbf{1.10}$$

$$\vec{v} = j\frac{e\vec{E}}{\omega m_e} \qquad \textbf{1.11}$$

With this basic foundation for a single electron, one can generalize the behavior of n_0 electrons per unit volume by examining the induced current per volume $\vec{J}$ and

Maxwell's Equations. The current density $\vec{J}$ is a measure of the current flowing through a cross-sectional area per unit time. Therefore, the units should be amperes per area. Eq. **1.12** shows this as the rate (velocity) that a given charge per volume is flowing. Replacing the velocity vector with Eq. **1.11** yields Eq. **1.13**.

$$\vec{J} = -en_0\vec{v} \qquad \textbf{1.12}$$

$$\vec{J} = -j\frac{n_0 e^2 \vec{E}}{\omega m_e} \qquad \textbf{1.13}$$

The extended form of Ampere's law from Maxwell's equations is stated in Eq. **1.14** where $\vec{H}$ is the magnetic field, and $\vec{D}$ is the electric displacement field. Neglecting the effects of polarization density, the electric displacement field is equivalent to $\varepsilon_0\vec{E}$ where ε_0 represents the permittivity of free space. Eq. **1.15** is the result of substituting $\varepsilon_0\vec{E}$ into $\vec{D}$ and performing the partial derivative (using the phasor form of $\vec{E}$ from Eq. **1.9**).

$$\nabla \times \vec{H} = \vec{J} + \frac{\partial \vec{D}}{\partial t},\ \vec{D} = \varepsilon\vec{E} \qquad \textbf{1.14}$$

$$\nabla \times \vec{H} = \vec{J} + j\omega\varepsilon_0\vec{E} \qquad \textbf{1.15}$$

Substituting the equation for current density found in Eq. **1.13** into Eq. **1.15** and isolating common terms yields Eq. **1.16** .

$$\nabla \times \vec{H} = j\omega\varepsilon_0\left(1 - \frac{n_0 e^2}{\omega^2 m\omega\varepsilon_0}\right)\vec{E} \qquad \textbf{1.16}$$

The term in the parenthesis is the dielectric constant, κ, of the plasma. It can be simplified to

$$\kappa = 1 - \left(\omega_{pe}^2 / \omega^2\right) \qquad \textbf{1.17}$$

where ω_{pe} is identical to Eq. **1.4** for the plasma frequency. This result shows that the propagation of an electromagnetic wave through the atmosphere is directly affected by the density (and therefore the frequency) of the atmospheric plasma.

The above derivations now yield sufficient information to approximate the propagation of a plane wave in the atmosphere. The propagation constant for this plane wave is e^{-jkz}. The wave number *k* is $\omega\sqrt{\mu_0\varepsilon}$ and $\varepsilon = \kappa\,\varepsilon_0$. The propagation constant can then be rewritten as $e^{-j\left(k_0\sqrt{\kappa}\right)z}$. Using Eq. **1.17** as the definition for κ, the following three cases for the propagation constant in the atmosphere are possible for a given signal of frequency ω:

(1) $\omega > \omega_{pe} \rightarrow 0 < \kappa < 1$

(2) $\omega = \omega_{pe} \rightarrow \kappa = 0$

(3) $\omega < \omega_{pe} \rightarrow \kappa < 0$

The first case is the standard form of a propagating wave. As a wave with an oblique incidence on the plasma propagates through a plasma with increasing n_0, κ will decrease and the wave will be bent downward. In the second case, κ is zero which corresponds in a backwards reflection of the wave. These first two cases combined show that a propagating wave will be refracted until a point in which the plasma frequency matches the frequency of the propagating wave. At this point the plasma reflects the

wave. If the frequency of the propagating wave is always higher than the plasma frequency, it will not be reflected by the ionosphere and continue propagating into space.

In the third case, the negative radical under the square root results in a positive and negative imaginary root. Choosing the negative root yields $e^{-jk_0(-jn)z} = e^{-nk_0 z}$ for some real and positive *n*. This is an evanescent wave rather than a propagating one. The alternative positive root yields a wave that increases exponentially. This is not a physically realizable solution as no mechanism exists for adding energy to the signal.

The previous section introduced the concept of collision frequency. The $-vm\frac{d\vec{x}}{dt}$ term used to account for collision frequency (where ν is the collision frequency, not velocity) adds a first-order term to the original differential equation, Eq. **1.3.** The solution to this equation, shown in Eq. **1.18**, is a more accurate representation of plasma frequency and accounts for the effects of high collision rates in the lower atmosphere.

$$\kappa = 1 - \frac{\omega_{pe}^2}{\omega(\omega - jv)} \qquad \textbf{1.18}$$

Eq. **1.18** shows that waves propagating close to the collision frequency will be severely attenuated. If collision frequency is zero, the imaginary term goes to zero and the original equation for plasma frequency is left.

1.3 Past Work and Contributions

This plasma frequency probe design builds on past work completed at Penn State. The electronics design of this experiment draws from the accomplishments of the Hybrid

Plasma Probe (HPP) development effort for Penn State's nano-satellite, LionSat. The HPP utilizes a PFP in conjunction with a Fast Temperature Probe and Swept-Bias and Fixed-Bias Langmuir Probes and common boom system. Specific contributions include the electrometer and the filter and transformer design after the direct digital synthesizer. [site Siegel, wyland] --expand on this

Chapter 2

Experiment Electronics

The Plasma Frequency Probe (PFP) is a self contained experiment. That is, all relevant electronics are located within the probe structure. The electronics layout utilizes a modular design—each subcomponent uses a dedicated printed circuit board (PCB) then all the boards stack vertically together. Board-to-board connections rely on a stackable header that creates a shared bus through each board.

The design for the stackable headers was adapted from the PC/104 industry standard for embedded computing. Due to size constraints and low demand for excessive board-to-board connections, the PFP uses a single 40-pin (2 rows of 20 pins) instead of the standard 104-pin bus which gives the standard its name. Four stand-off screws designed for the height of the stacking connectors separate each board. The stack of fastened boards then mounts inside the probe's lower shaft.

A modular design has certain advantages. First, for development and testing, it is much easier to debug individual smaller circuits rather than one large one. Each board

acts as a stand-alone experiment the experimenter can test individually. This way, a problem with a single board cannot delay the entire design. With the entire design broken into smaller components, development can proceed in a parallel process, rather than a serial one. This engineer realized this benefit in the preparation of the experiment. When problems began to arise in the first revision of some of the experiment boards, development of the rest could continue regardless.

Finally, modular design aids grounding techniques. In the design process, board designers often overlook grounding strategies. Ground problems are heavily documented as being a cause for significant circuit errors. Utilizing separate ground planes reduces noise from one part of the experiment corrupting the others.

2.1 Power Board

The PFP draws its power from a BWR-15/575-D24A model DC to DC converter manufactured by Datel. This single package measures 1.0 x 2.0 x 0.48 inches and provides dual ±15 volt outputs at 17 watts total from a single 18 to 36 volt input. The single input, dual output feature is especially relevant to the integration into the SPIRIT payload as the payload power system had a shortage of power relays. There were not enough relays for the power system to supply two voltages. Refer to section **3.3** for further explanation of the power system interface.

The converter regulates the power outputs and provides a separate isolated ground from the payload power bus. Effectively isolating the PFP circuitry from the payload bus removes unwanted external noise corruption from the payload power bus.

Final testing shows that the PFP requires at most 220mA from either supply voltage. This requirement is less than 40% of the maximum capability of the DC/DC converter. Early estimates of the experiment power consumption required a power board capable of supplying at least 350 mA. The current power board design satisfies this requirement with a significant factor of safety. In fact, to ensure the stability of the DC/DC converter, the design includes load resistors that pull a total of 120 mA. Future designs of this experiment could reduce current requirements to around 100 mA for the entire experiment with an appropriately sized power board.

In contrast to linear regulators which dissipate unnecessary power as heat, these DC/DC converters are switched mode power supplies that are between 84%-86% efficient[reference datasheet]. These efficiencies translate to lower thermal power dissipation and reduced requirements from the batteries.

Linear regulators produce a lower output voltage by dividing the input voltage according to an internal reference. The voltage drop from the input to output voltages dissipates across a transistor or other device. The linear regulator dissipates this power ($I_{out} \bullet \Delta_{Vin-Vout}$) as heat.

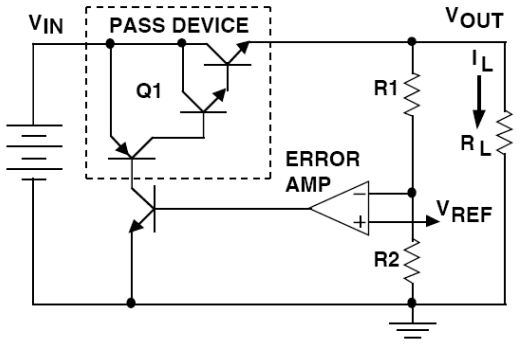

Figure **2-1**: Linear Regulator Simplified Schematic

This is a concern especially for applications in vacuum environments (which this application is by virtue of being a space payload instrument). Without ambient air to dissipate the heat, convection cooling does not exist. Therefore the regulator must dissipate the heat through the PCB (which may heat other parts soldered to it) and throughout the regulator itself. Depending on the voltage drop, this can be dangerous.

For instance, using the alternative design of voltage regulators, the payload power system would supply this instrument with a nominal +18V power line (which could be as high as 22V) to supply +12V and +5V at 350 mA. Eq. **Equation 2.1** shows the thermal energy generated.

$$\begin{aligned} 0.350\,amps \times (22\,volts - 12\,volts) &= 3.5\,watts \\ 0.350\,amps \times (12\,volts - 5\,volts) &= 2.45\,watts \\ Total &: 5.95\,watts \end{aligned}$$

Equation 2.1

The payload would also have to supply an additional -18V power line as linear regulators cannot invert voltage.

Figure **2-2** illustrates the operation of a DC/DC converter. In contrast to linear regulators, DC/DC converters like the one used with the PFP are switched mode power supplies. They operate by applying the DC input voltage across a transformer, storing magnetic energy, then switching it off and transferring the energy to the output. The device regulates the output voltage using pulse width modulation (PWM). In other words, the device control circuitry adjusts the duty cycle of the on/off pulses according to the control circuitry in order to provide the desired output. The switching operation, rather than just dissipating the extra power, is the reason for higher efficiency. This device also produces a bipolar (both a positive and negative) voltage supply from a single

positive input that can range from 18V to 36V with no impact on the design. The outputs are isolated from the inputs up to $1500V_{DC}$.

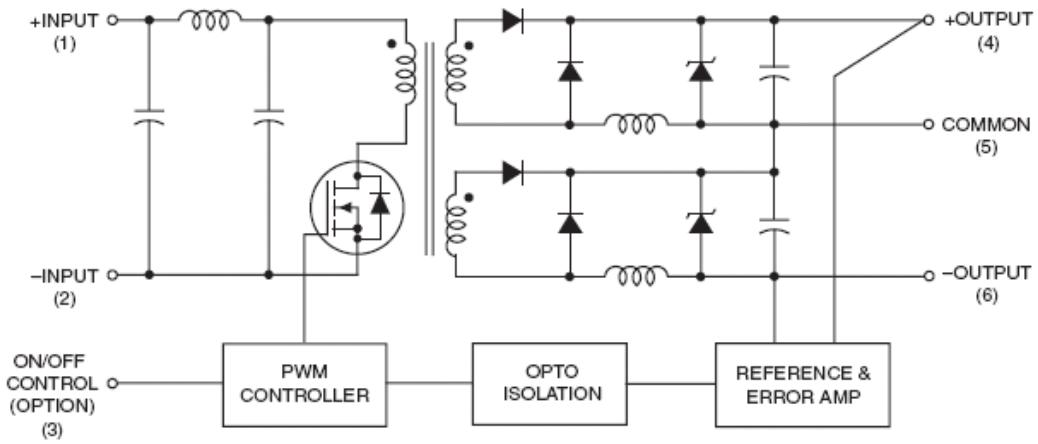

Figure **2-2**: Datel BWR-15 DC/DC Converter simplified schematic

The switching frequency used by the BWR-15 model is 300 kHz (±30 kHz). While this switching operation improves the efficiency and reduces the thermal dissipation requirements, the switching can cause noise on the power supply lines throughout the circuit.

The Datel specifications indicate that no external components are required. However, analysis of the output on an oscilloscope showed significant ripple up to TBD V peak-to peak. Analysis using a spectrum analyzer confirmed that the noise occurred at the switching frequency and harmonic frequencies thereafter. While this noise may be acceptable for some designs, additional filtering on the PFP boards reduces this ripple significantly. [describe filtering topology, cutoff frequency, spectrum analyzer results, output results]

A final requirement DC/DC converters have for stability is that the supplied circuitry draws a minimum percentage of the maximum available current. The BWR-15/575 part sets this minimum to 10% or 57.5 mA. To guarantee the power board meets this condition, it includes a 250Ω, 35W power resistors on each supply line to draw 60 mA.

The PFP uses the same grounding technique as the SPIRIT payload itself—that is, the star ground technique. Ideally all signal returns connect to a single, or star, ground. In reality, this is not always practical. A solution is to have each subcomponent have a local star ground and then each of these nodes eventually connect together. By using modular designs, each circuit is able to use separate ground planes, copper pours, or star nodes. All boards then connect to the respective analog or digital ground through the common stacked experiment bus. All ground nodes eventually return to the power board, completing the circuit.

The accelerated development pace of this project required the development of the power board in parallel with other components of the instrument. As such, the board incorporates a large factor of safety in the capacity it can provide. The BWR-15/575 DC/DC converter is capable of sourcing 575 mA on each of the ±15V supply lines. This is more than the 220 *mA* current required for the positive supplies and certainly more than is required by the negative supplies. Future designs should use power supplies tailored to the needs of the application. Appropriately sized power supplies will further increase the efficiency of the design and reduce the power requirements of the payload power bus.

To test the ability of the power board to operate in the vacuum conditions of space, a vacuum test was performed on the board using vacuum chambers at NASA's

Wallops Flight Facility. The vacuum chamber simulates the space environment by reducing the pressure inside the chamber containing the power board to 250,000 *feet* while drawing more than the expected current needed during flight. A pass-through connector allows for wires to pass from inside the chamber to the outside. A power supply external to the vacuum chamber provides the +28V to the board while an external electronic load ensures that 300mA is continuously drawn from each of the ±15V power outputs. Throughout the test, digital multi-meters periodically measure the ±15V outputs from the DC/DC converter and the ±12V and ±5V regulators to ensure regulation is constant. Additionally, thermocouples constantly monitor the temperature of the DC/DC Converter, two 200Ω load resistors, +5V regulator, -5V regulator, and +12V regulator. Figure **2-3** and figure **2-4** illustrate the results below.

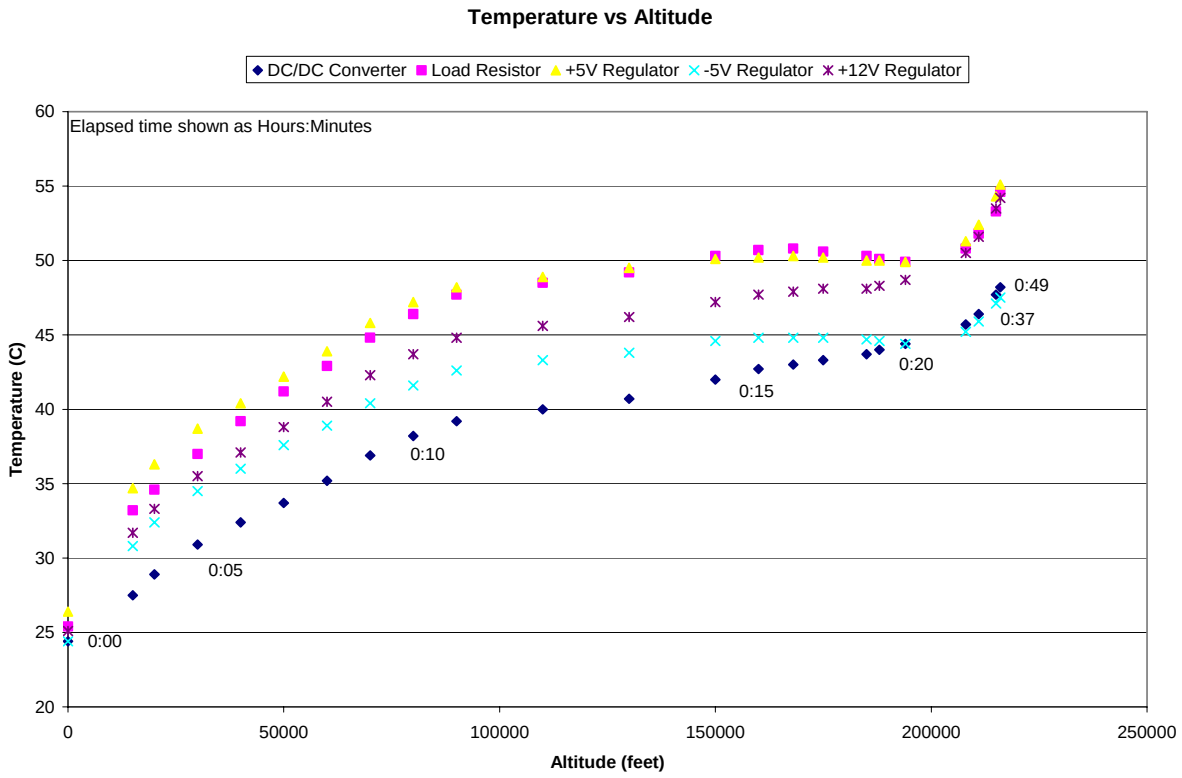

Figure **2-3**: Power Board Vacuum Test: Temperature vs. Altitude

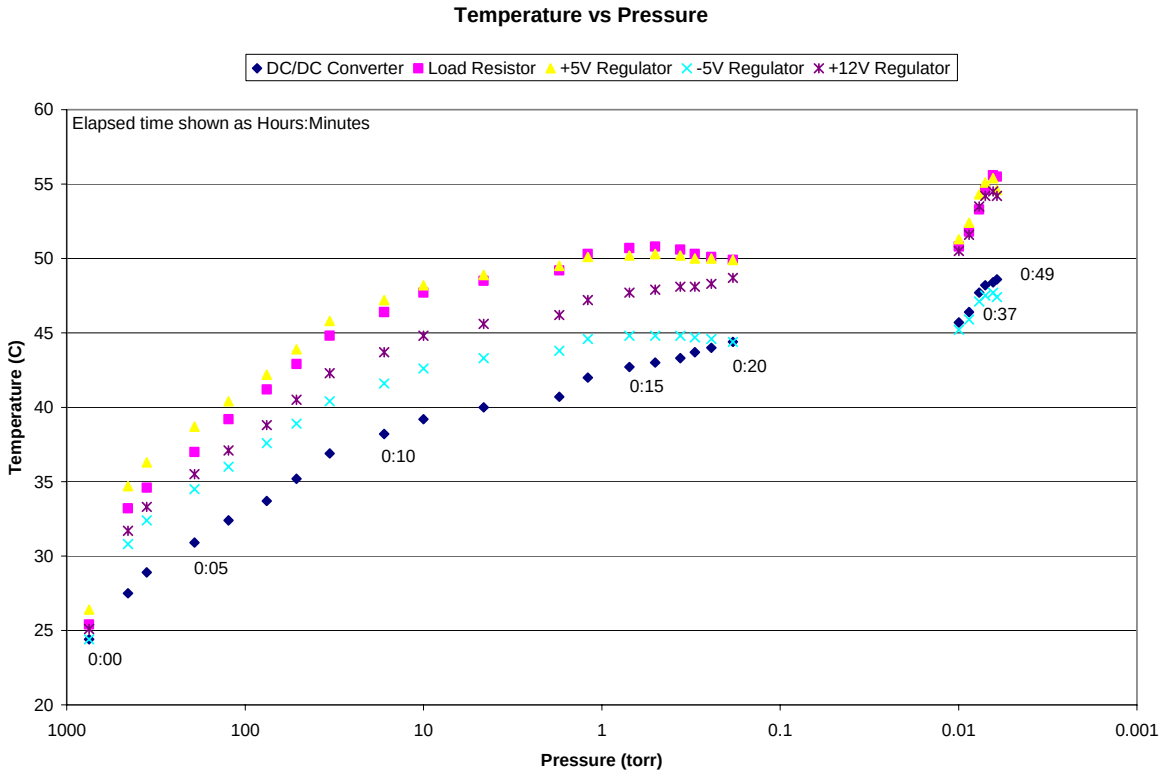

Figure **2-4**: Power Board Vacuum Test: Temperature vs. Pressure

2.2 Housekeeping and Payload Interface Board

The Housekeeping and Payload Interface Board monitors the ±5V and ±12V supplies used by each of the experiment boards. It measures current supplied to the DC/DC converter. These sensors are vital to monitoring performance during flight but also during pre-flight integration and testing in the ground station and on the launch rail. The positive voltage monitors are simple buffered voltage dividers with gains of approximately 0.5 and 0.208 for the +5V and +12V supplies respectively. The nominal output is then 2.5V to the PCM. The negative voltage monitor uses the same voltage

dividers but with an inverting operational amplifier with unity gain. Similar to the positive monitors, these outputs to the PCM are also 2.5V.

The current sensor uses a Sentron CSA-1V Hall-effect integrated circuit chip manufactured my GMW Associates. Hall-effect sensors measure current indirectly by measuring the magnetic fields that the current-carrying wires radiate. The advantage of these chips is their passive measurement. Unlike other designs, the measuring circuit does not interrupt the wires it is measuring. The chip manufacturer recommends two distinct PCB layouts, shown below in Figure **2-5**, depending on the target current to measure. The image on the left accommodates currents less than 2A and yields a sensitivity of 460 *mA/V*. The image on the right accommodates up to 8A and yields a sensitivity of 38 *mA/V*. For the lower current supply of the PFP, the housekeeping board uses the layout design illustrated in the left image. An amplifier at the output of the CSA-1V chip further reduces or increases the final gain as needed.

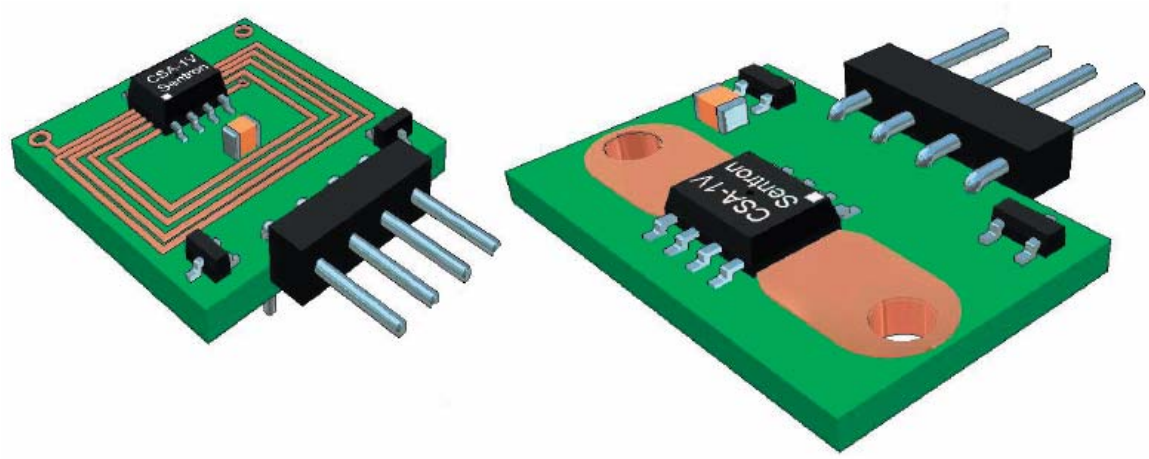

Figure **2-5**: PCB Layouts for Sentron Hall-Effect Current Sensors

2.3 Digital Control Board

The digital board includes all the digital circuitry for the experiment. This includes the MC9S12C32 microcontroller (hereafter referred to simply as HCS12) from Freescale Semiconductor (formally Motorola), and the AD9834 Direct Digital Synthesizer (DDS) from Analog Devices.

There are many choices of microcontrollers. The PFP design adopted the HCS12 because of its history in early development efforts and easy interface using the Code Warrior Integrated Development Environment software from Metrowerks. The HCS12 package includes Serial Peripheral Interface (SPI), Serial Communications Interface (SCI), and enough on-board flash memory to store the required code. The DDS requires the SPI block for control of the DDS and the SCI block provides asynchronous communication to the telemetry encoder to record what step of the frequency sweep the microcontroller sends to the DDS.

Furthermore, a small HCS12 module was available for purchase from Axiom Manufacturing that serves as a plug-and-play solution. It was determined that the cost of these modules, shown below in Figure **2-6**, was easily more cost- and time-effective than developing a new circuit. The module includes a 40-pin connector that simply solders into the digital board (a different connector from the common header shared by all the boards).

Figure **2-6**: MC9S12C32 Module

Axiom designed the module as a development board. As such, it includes push buttons, jumper-selectable power options, an extra power receptacle, LEDs, and a 9-pin D-Sub connector for asynchronous communication. None of these options are necessary. In fact the DSUB, external power connector, and jumpers are too tall for the minimum board-to-board spacing. Also, the reset push-button has a potential to inadvertently trigger from in-flight vibrations. As such, the flight version of this module, shown below in Figure **2-7** has all of these superfluous components removed

Figure **2-7**: Modified HCS12 Module

As referred to above, the first function the HCS12 must serve is the control of the Analog Device's AD9834 DDS.

The DDS (shown in **Figure 2-8** below) is a numerically controlled oscillator. It is similar to a conventional voltage controlled oscillator (VCO) except that the DDS output

is controlled, or tuned, by the serial digital input from a microcontroller. The DDS contains three types of data registers: control, frequency and phase. After power-on, the serial input first writes to the control register to initialize the chip and to reset the frequency and phase registers. Following initialization, subsequent writes to the frequency register set the output frequency. A single update to any register requires a 16-bit word. Phase registers are not required for this experiment and are set to zero.

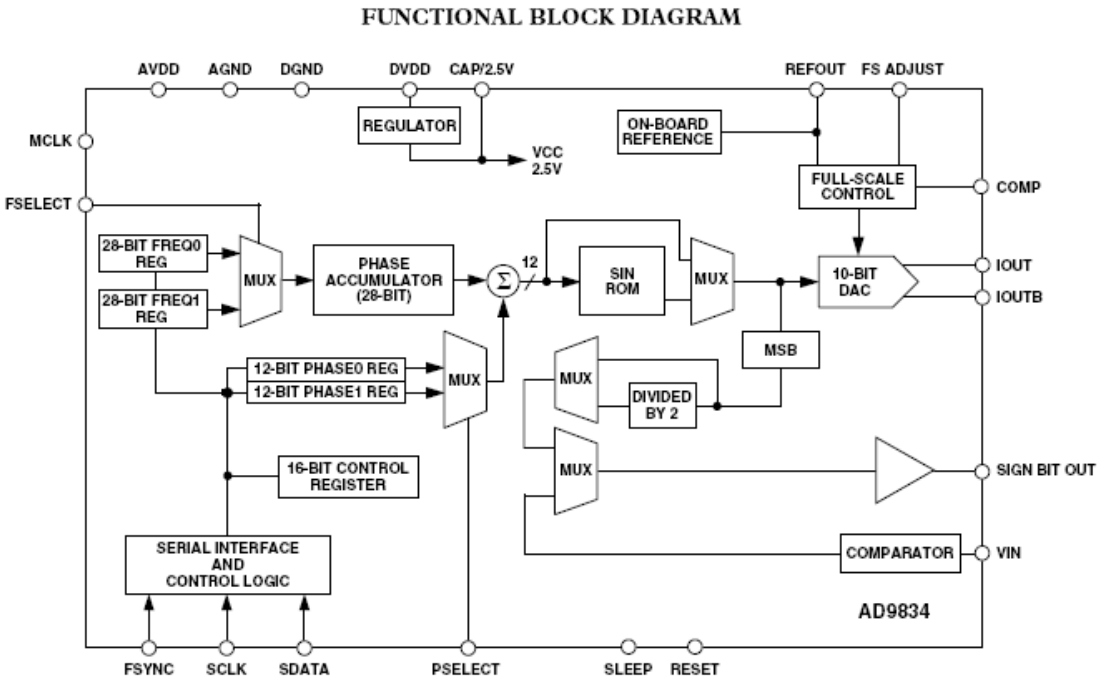

Figure **2-8**: Functional Block Diagram of the AD9834 Direct Digital Synthesizer

The PFP uses four of these distinct blocks to generate the necessary sinusoidal waveforms. These are: the 28-bit FREQ0 register, NCO (28-bit phase accumulator), SIN ROM, and 10-bit DAC. The AD9834 operates on the principle that angular position of a sinusoidal wave linearly relates to the unit time. Rather than calculate the result of $sin(\omega t)$ using complicated processing, the chip begins with calculating the phase angle

with the linear relationship $\omega = 2\pi f$. This DDS uses the 50 MHz external clock input as a reference, calculates the phase angle for that period, and then calculates ω.

$$\Delta phase = \omega \Delta t$$ **Equation 2.2**

$$\omega = \frac{\Delta phase}{\Delta t} = 2\pi f$$ **Equation 2.3**

Using this result and substituting the reference clock frequency for the reference period, the linear frequency, f, is found.

$$\frac{1}{f_{MCLK}} = \Delta t$$ **Equation 2.4**

$$f = \frac{\Delta phase \times f_{MCLK}}{2\pi}$$ **Equation 2.5**

The numerically controlled oscillator (NCO) is capable of generating signals based on user inputs for two frequency registers and two phase registers. While these options provide powerful capabilities, the following section discusses only the single frequency register required for the PFP operation.

The NCO contains a 28-bit phase accumulator which allows for 2^{28} discrete values for phase between 0 and 2π. After 2π, a sinusoid repeats so a larger range is redundant. Substituting 2^{28} for 2π in Eq. **Equation 2.5** yields a new value for frequency.

$$f = \frac{\Delta phase \times f_{MCLK}}{2^{28}}, \quad for\ 0 < \Delta phase < 2^{28}$$ **Equation 2.6**

The next step in generating the sinusoid waveform is the SIN ROM block. The SIN ROM converts the phase data into the corresponding sinusoidal value by serving as a simple look-up table, using the phase data as a table index. Since the data eventually ends with a 10-bit DAC, the SIN ROM lookup table contains only 2^{12} entries—yielding two more bits of resolution than the DAC in order to overcome errors due to truncation. Using 2^{28} entries is unnecessary.

With the new values from the SIN ROM, the data is then passed to the high impedance current source 10-bit DAC which provides the final output from the chip. An external R_{SET} resistor sets the full scale output current of the DAC. The output can be either single ended or differential through the IOUT and IOUTB pins.

The *FREQ0* register sets the frequency of the analog output from the DDS. A single frequency register contains 28 bits of data and the microcontroller must update this register in two consecutive 16-bit writes. Each write to the chip contains either the 14 most significant bits (MSB) or 14 least significant bits (LSB) of the desired frequency. The remaining two bits in the 16-bit word are used to append the address of the register the write is designated for (frequency, phase, or control registers). The output frequency is determined by using the number represented by these 28 bits as a multiplier for a ratio of the input clock. The relationship is shown in **Equation 2-7:**

$$f_{OUT} = \frac{f_{MCLK}}{2^{28}} * FREQREG$$ **Equation 2-7**

The PFP uses a 50 MHz oscillator as the f_{MCLK} source. The frequency output is limited to $f_{MCLK}/2$ giving a frequency range of 0 *Hz* (*FREQREG* = 0x00) through 25 *MHz* (*FREQREG* = 0x800 0000).

Since the DDS generates its output by sampling the f_{MCLK} input, the output necessarily has harmonics of the output frequency that are mirrored images around the clock frequency. In other words, the output signal will contain noise caused by the harmonic image frequency caused by discreet sampling. These image frequencies are given by: Eq. **2.8**.

$$f_{image} = \left|\left(f_{MCLK} \times n\right) - f_{OUT}\right|, \quad n = \pm 1, \pm 2, \pm 3, \ldots \qquad \textbf{2.8}$$

These image frequencies decay in power following a $\frac{\sin(x)}{x}$ envelope. Therefore, the image frequencies only become significant as the output frequency approaches the 25*MHz* Nyquist rate. Figure **2-9** shows the superimposed spectral plots for four individual output frequencies. The desired output frequencies, f_1, f_2, f_3, and f_4, are 1*MHz*, 10*MHz*, 20*MHz*, and 25*MHz* respectively. As the desired output frequency approaches the 25*MHz* Nyquist rate, its mirror harmonic image similarly approaches 25*MHz* from the opposite direction with an increasing magnitude. There is no harmonic image shown for f_4 because its first harmonic is also 25*MHz*. In the time domain, this results in a clean sinusoidal output at lower frequencies, which begins to noticeably degrade after around 20*MHz*. The small peak between f_2 and f_3 is from the 16*MHz* microcontroller clock frequency.

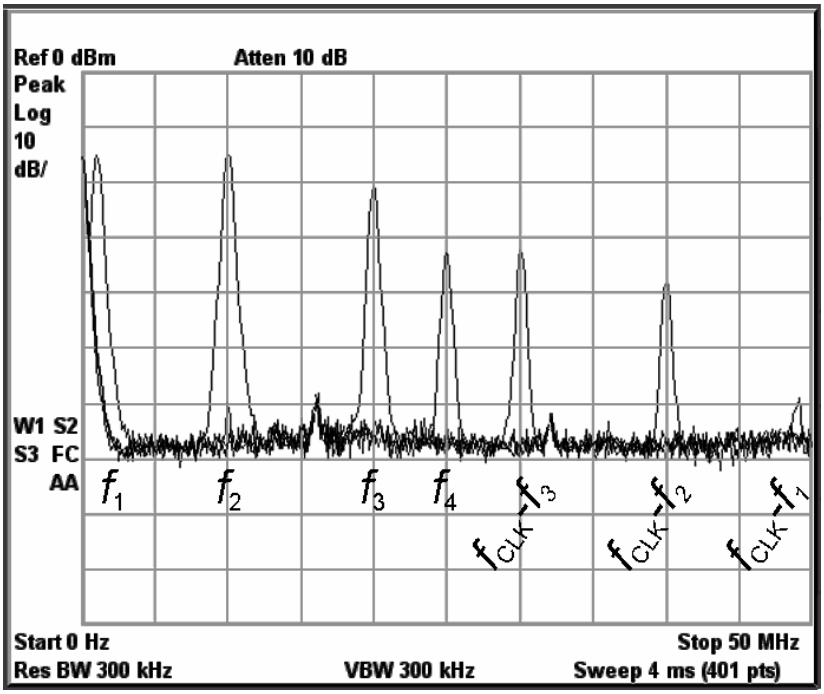

Figure **2-9**: DDS Spectrum Analysis

2.4 Analog Analysis Board

The Analog Analysis board sits at the top circuit stack includes connections to the probe and the phase and gain measurement circuitry. Figure **2-10** below illustrates the first part of the circuit. A single triaxial connector provides the three necessary connections. The outer shield is chassis ground, and is connected to the mounting shaft directly below the guard. The inner shield carries the drive voltage generated by the DDS on the digital board. It connects to the guard ring directly below the probe collection surface. The center conductor connects to the probe tip and collects the return current to compare with the control signal.

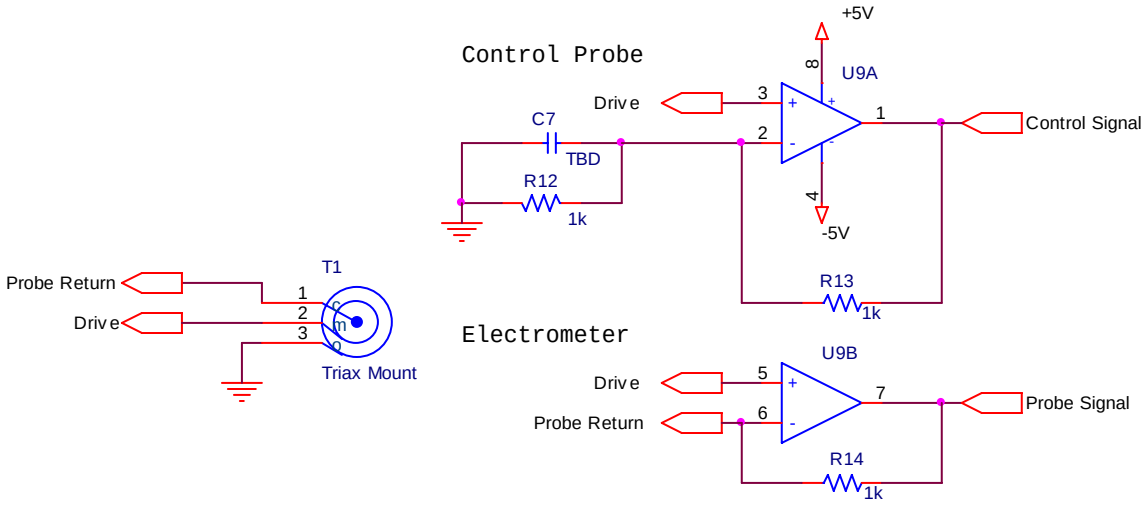

Figure **2-10**: Triaxial connector and electrometers

The voltage on the center conductor is the same as the one applied to the guard; however the guard and probe signals are not the same. An operational amplifier effectively copies the drive voltage to the probe-return signal through the terminals of an operational amplifier. The feedback resistor connected between the output and inverting terminal of the electrometer operational amplifier converts the return current to a voltage. The following detection circuitry uses this voltage in conjunction with the output voltage from the control probe to analyze the plasma impedance.

After the collection board converted the return currents to usable voltages, circuitry on the detection board analyzes the differences between the probe signal and the control signal. Detection of both phase and gain relies on the AD8302 2.7*GHz* RF/IF Gain Phase Detector (shown below in **Figure 2-11**) from Analog Devices. This signal chip incorporates both a phase detector and a dual logarithmic gain amplifier.

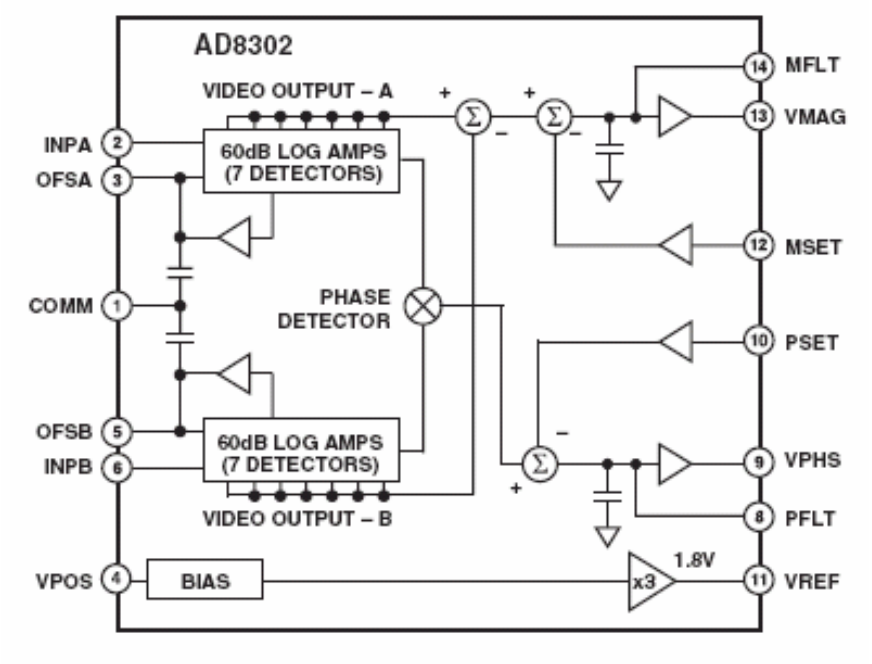

Figure **2-11**: AD8302 Gain Phase Detector Functional Block Diagram

The data sheet specifies dynamic operation between DC and 2.7*GHz*. However, after initial designs failed to work, this author discovered that the chip has an internal high-pass filter with a cut-off frequency of 200*MHz*. Luckily, the chip allows designers to add extra capacitance to the filters via the *OFSA* and *OFSB* pins to lower the cut-off frequency below 100 *kHz*—the minimum range of the experiment. **Equation 2-9** is the equation for the high pass filter.

$$f_{HP}(MHz) = \frac{2}{C_C(nF)} \qquad \textbf{Equation 2-9}$$

C_C represents the total capacitance between the offset pins, *OFSA* or *OFSB*, and ground. This capacitance includes an internal 10 *pF*. Therefore, solving for $f_{HP} = 0.5\ MHz$ yields a value for C_C of approximately 4 *nF*.

With extra capacitance added to the *OFSA* and *OFSB* pins, both phase and gain components of the chip worked as expected. The device was tested using two Agilent 33120A Waveform Generators equipped with the Opt001 addition. This addition allows the two generators to be phase-locked. The output from the first generator was connected to Input A of the AD8302 and held at a fixed phase. The output of the second generator was connected to Input B and then the phase was swept. The results of the first prototype of the AD8302 design are illustrated in Figure **2-12 and** Figure **2-13** below.

The AD8302 is the most accurate and reliable phase and magnitude design to date. However, one drawback exists. The phase detector is only capable of detecting the absolute phase difference.

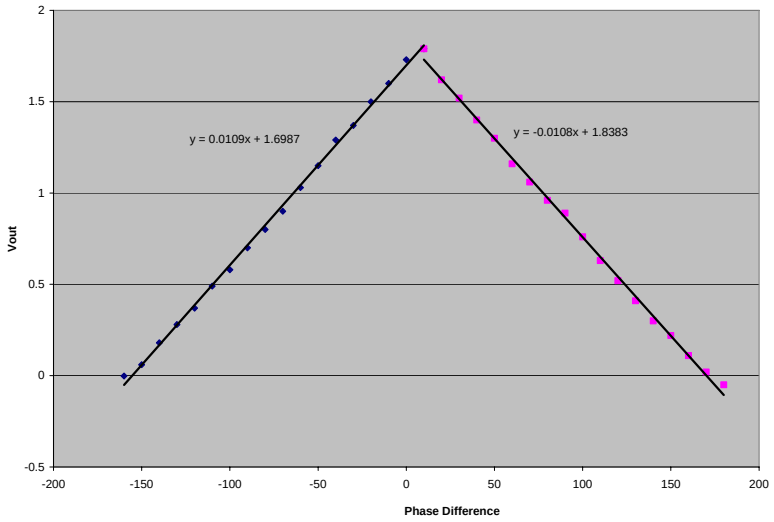

Figure **2-12**: AD8302 Phase Detection Preliminary Data

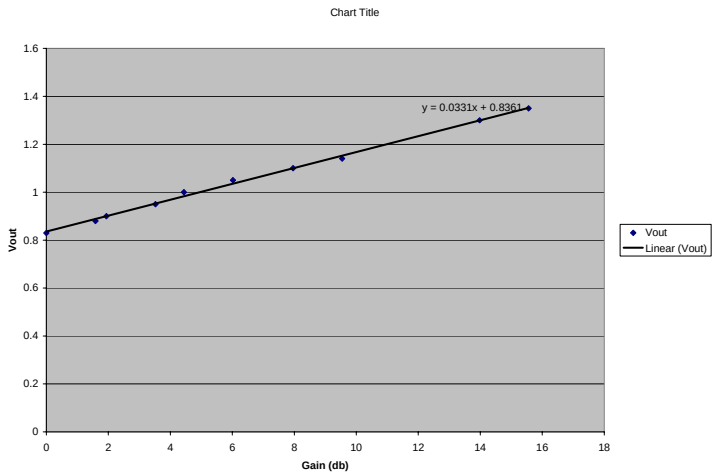

Figure **2-13**: AD8302 Magnitude Detection Preliminary Data

Chapter 3

Subsystem Interface

The Plasma Frequency Probe is just one experiment that comprises the SPIRIT III payload. Each experiment must interface with the payload power system, telemetry system, and the payload mechanical structure. The following sections describe these interfaces.

3.1 Structural System

At the onset of the SPIRIT program, a trade study analyzed whether to use booms or a type of nose-tip probe. A Langmuir probe experiment required the use of two booms on the forward section of the payload. If the PFP was to use booms, they would have to

either mount on the forward bulkhead with the Langmuir probes or mount on the aft bulkhead of the payload and deploy after the second stage booster rocket separates. After a study of the payload layout, the structures team determined that the proximity of the lower bulkhead to the booster is too close to use booms. The deployment of two extra booms on the forward bulkhead reduces the angular momentum of the payload enough to threaten stability. This reduction of angular momentum contributes to unwanted coning of the entire payload.

With booms no longer an option, a nose-tip probe similar to one most recently flown on the MacWAVE PFP experiment conducted by Robert Siegel (and croskey/bilen/wyland?). <<explain history>>. This probe is shown below.

<<<<insert rob's probe>>>>

Figure **3-1** below illustrates the final probe structural design as a part of the entire SPIRIT III payload. The probe consists of three aluminum parts, each separated by three Delrin® insulators. Strictly speaking, the probe used to collect data consists only of the farthest most aluminum component: the hemispherical tip and corresponding cylindrical mount. This gives a large, smooth surface area that maximizes contact with the atmospheric plasma. The middle ring, or guard, minimizes any discontinuities, and has the same voltage applied to it as the collection probe, but is not used for collection itself.

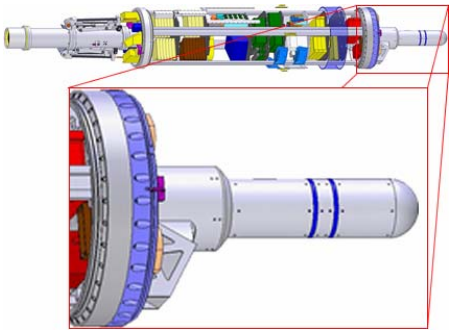

Figure **3-1**: CAD Illustration of the PFP

The collection probe and guard are gold-plated to improve electrical properties of the collection surface.

Finally, the lower shaft provides the mechanical connection to the rest of the payload connects electrically to the experiment ground. The mounting shaft design allows the collection surface to be as far removed from the payload as possible. The added benefit of this extra space is that all the required circuitry fits inside the probe structure. As mentioned above, the PFP is completely self-contained with no supporting equipment inside the main payload. Similar to the methodology of the modular circuitry, the PFP itself can be easily detached from the main payload by unfastening six screws and a single electrical connector. This way engineers can perform development, integration, testing, and initial calibration without any other payload components.

3.2 Telemetry System

The nature of SPIRIT's non-recovered sub-orbital sounding rocket mission excludes any type of on-board data logging equipment. Therefore, the experiment must relay all data through the telemetry system to ground tracking stations in near-real time.

The SPIRIT III telemetry system encompasses two major components: the pulse code modulation (PCM) encoder and the transmitter. The PCM encoder acts as the interface to all the data signals in the payload. The encoder accepts both digital and analog inputs. Digital interfaces include RS-232 and parallel data. Any experiment or monitor sending analog signals to the encoder scales the signal from 0-5V. Analog to digital converters inside the encoder then convert each analog channel into 10-bit words sampled at a sampling rate determined by the experimenter and limitations of the encoder. The discrete voltage steps are all equal and are calculated using **Equation 3-1**

$$V_{step} = V_{swing} * \frac{1bit}{N\,bits} = 5V * \frac{1}{4095} = 1.221mV \qquad \textbf{Equation 3-1}$$

Therefore, all flight data can only be resolved down to 1.2 mV intervals. For experiments requiring higher resolution, the experiment digitizes the data locally and then sends it to the PCM encoder in multiple digital words. Once all channels are in digital form, the encoder multiplexes them into a single bit-stream and sends them to the transmitter.

For the plasma frequency probe specifically, the simplest data-transfer solution, at least from the experimenter's side, is simply to record the data output from each electrometer. This would remove any need for detection circuitry. However, with

discrete sampling, the encoder samples the signals at least at the Nyquist rate to ensure valid data. Since each output contains frequencies up to 10 MHz, this translates to more than 20 million samples per second.

The SPIRIT payload is using an encoder with a total allocated data rate of 1.5 Mbps. Using 10 bits per sample translates to 150,000 samples per second. The SPIRIT payload must relay more than 100 channels through this single encoder. This requires that each experiment reduce sampling rates to a minimum. With these constraints, sampling the raw 100 kHz – 10 MHz electrometer waveforms requires too much bandwidth to be practical. For this reason, phase and magnitude detection is performed in-situ. The analyzed results require significantly less bandwidth.

The PFP generates three data channels. The first is a digital word in RS-232 format that indicates which frequency step the experiment is currently on. The sweep consists of 255 logarithmically spaced frequencies between 0.1 to 10 MHz.

The two remaining channels are analog and represent the measured differences in phase and magnitude. The rate of the frequency sweep determines the sampling rates required, not the frequencies in the sweep itself. This reduces the telemetry requirements to thousands of samples per second rather than a millions.

The analog channels connect to the telemetry encoder along with a ground reference wire. This reference is the signal ground connected to the COM pin on the DC/DC converter. This is necessary because the PFP is using a different voltage reference via the isolated DC/DC converter. Also, any noise induced on the signal lines from other sources in the payload between the PFP and the encoder will also corrupt this

ground reference. With identical noise on the signal and the reference, the effect cancels out.

3.3 Power System

As described in section **2.1**, the payload power system must supply the PFP experiment with a nominal +28V at 350 mA for the duration of the flight and the time required to provide payload pre-flight checks before launch. Payload power flows from one of two sources: internal primary batteries or external power supplies supplied through an umbilical connector between the payload and the ground station. The ground station switches from internal to external power by controlling relays inside the payload using control lines in the payload umbilical. Because of the shortage of payload power relays, the PFP uses a single voltage supply and creates bipolar outputs with a DC/DC converter rather than use a positive and negative supply from the payload.

The PFP experiment has a wide input range. Therefore the input voltage can deviate from the nominal voltage to as low as +18V or as high as +36V. The power wire is twisted with its return to the battery to minimize noise.

Chapter 4

Analysis and Results

Start here

4.1 Calibration Data

Start here

4.2 Procedure for Post-Flight Analysis

Start here

Chapter 5

Improvements for Future Designs

Constructing an experiment for a rocket payload requires adherence to strict deadlines. While there are always ways to make the design better, there comes a point when design engineers must freeze the designs in order to progress towards the final revision. The following section outlines methods for improvement that future experimenters may use to build the next generation of Penn State's Plasma Frequency Probe.

5.1 New Theory of Operation

Reflectometer, would remove need for +12V

5.2 Additional Phase information

Add sign of phase information

5.3 Redesign of Power Board

Make +/-5V, size to current needs of experiment, add filtering

5.4 Redesign of Probe Structure

Make smaller?

Bibliography

This paragraph is the default "BibliographyEntry" style layout with an example *BibliographyEntryTitle* style illustrated within.

Collins, R. (1985). *Antennas and radiowave propagation*. New York: McGraw-Hill Inc.

Incomplete . .

Appendix A

Electrical Schematics

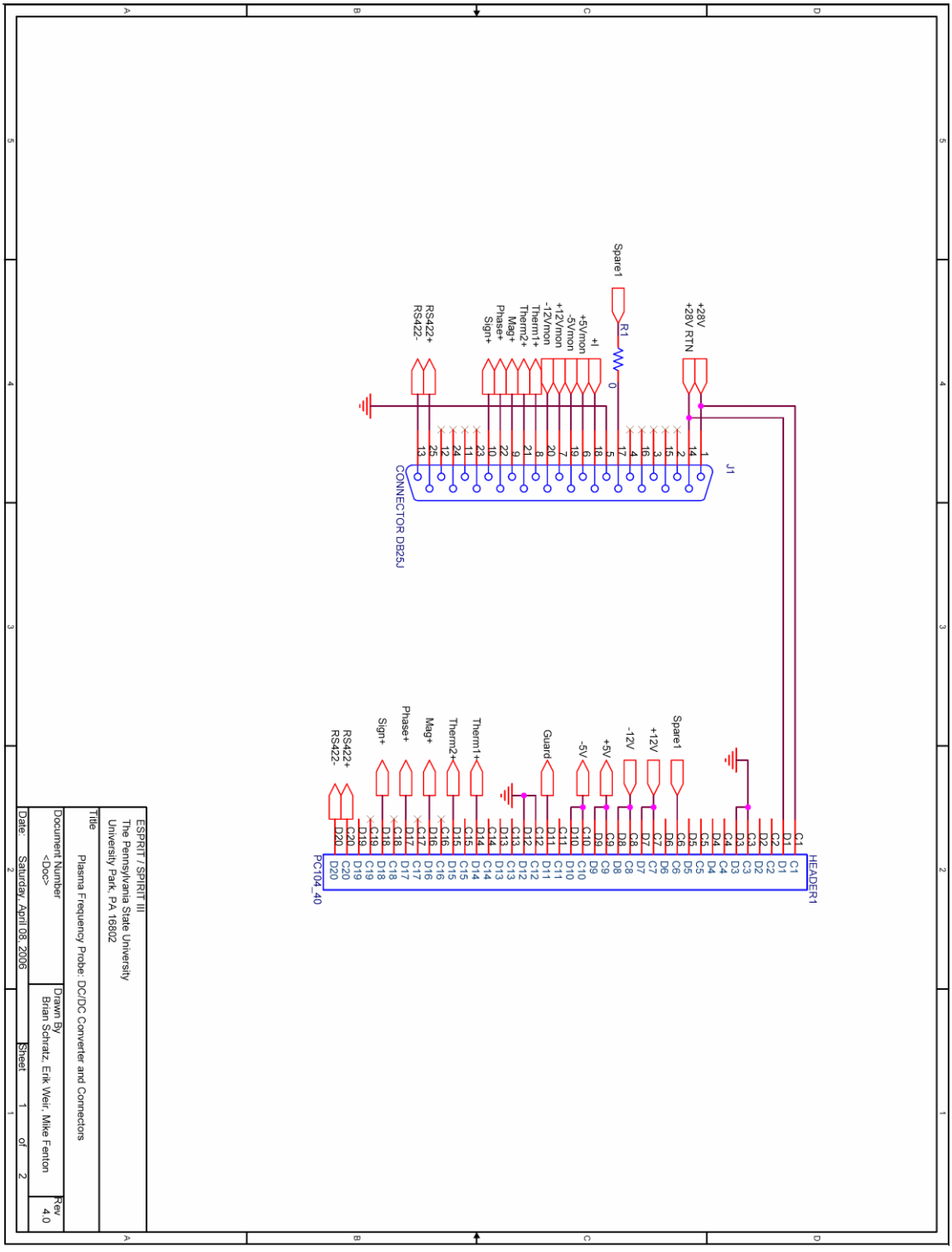

Figure **A-1**: Housekeeping Board: Instrument Bus and Payload Interface

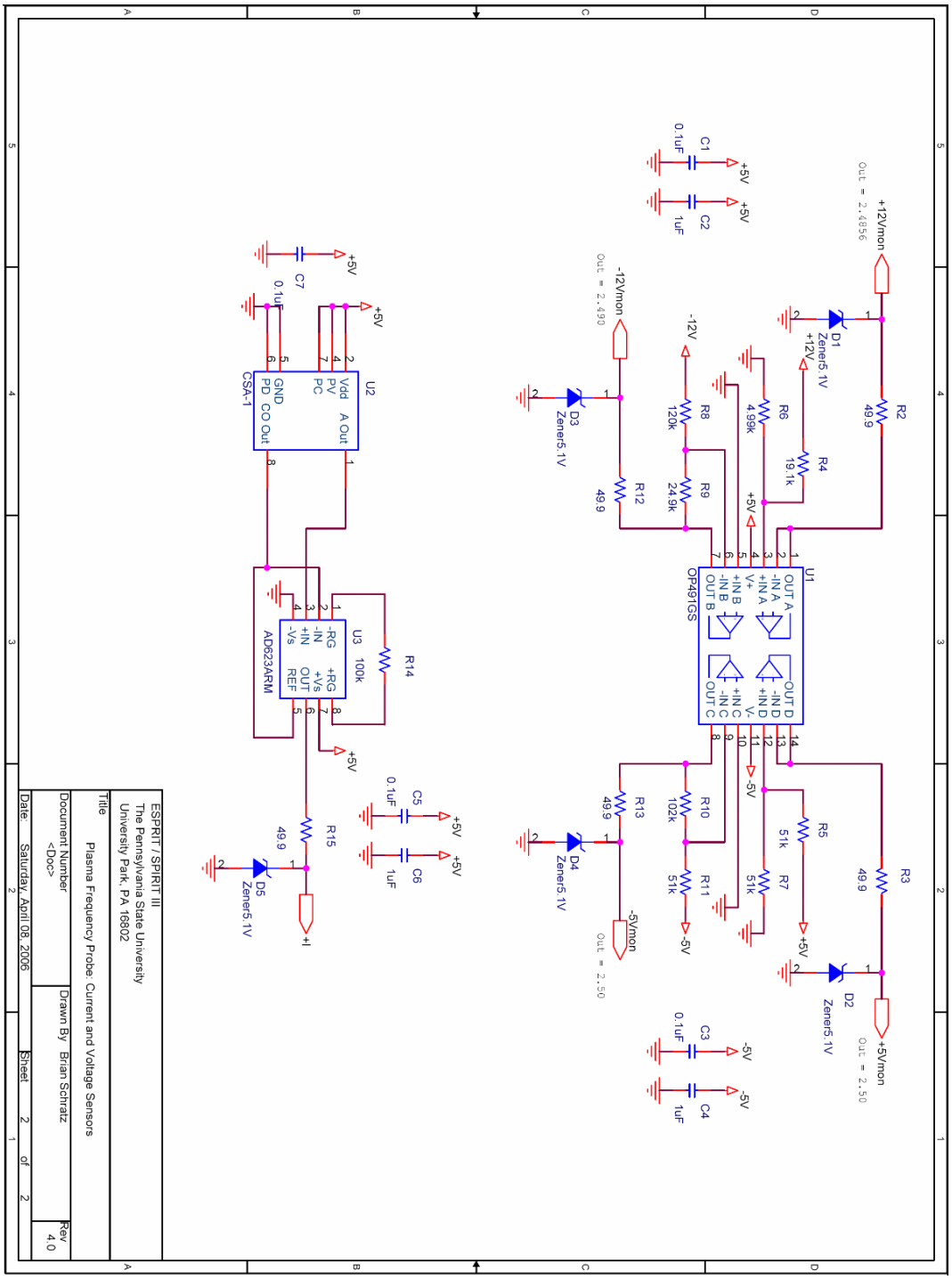

Figure **A-2**: Housekeeping Board: Voltage and Current Sensors

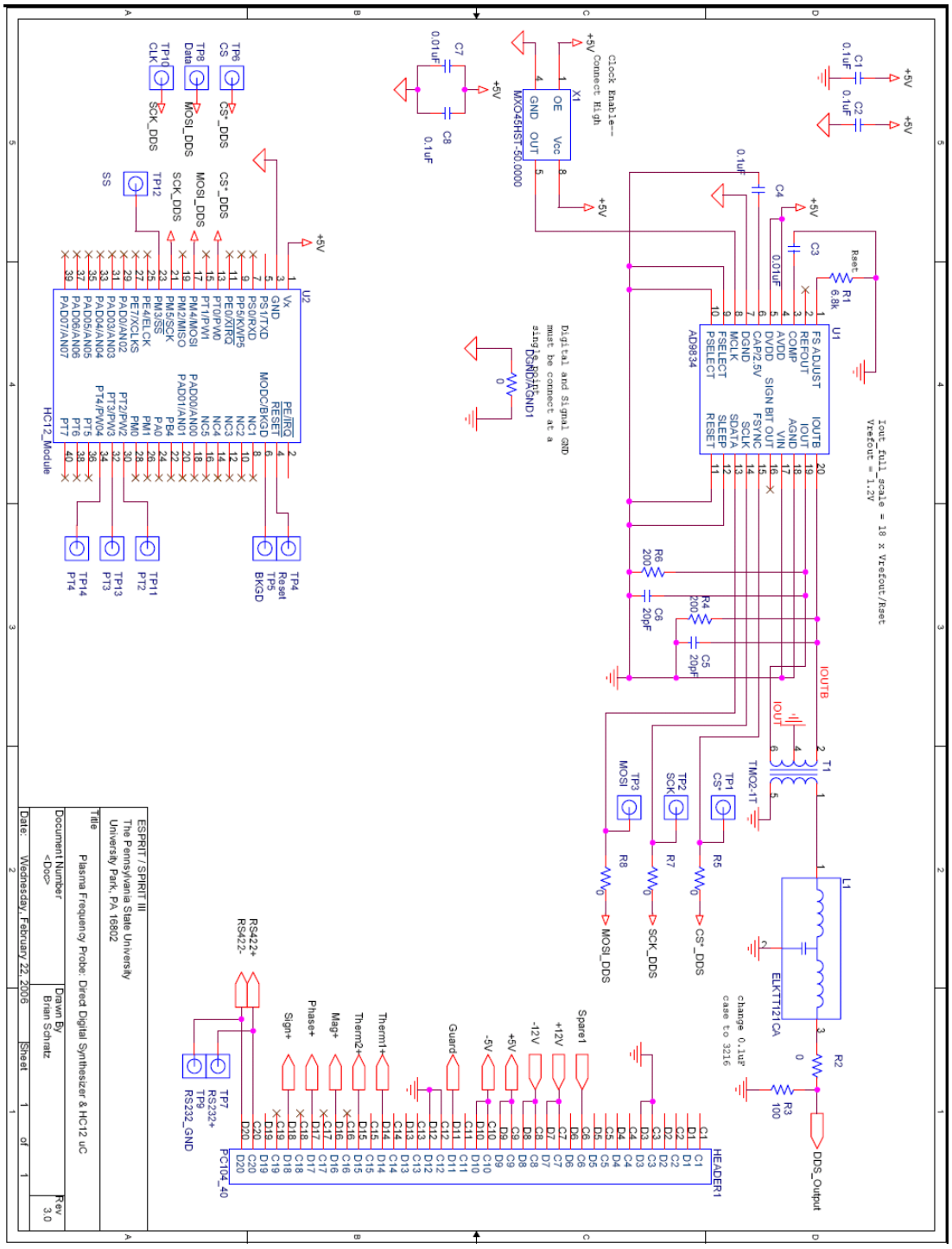

Figure **A-3**: Digital Board: DDS and Microcontroller Module Connection

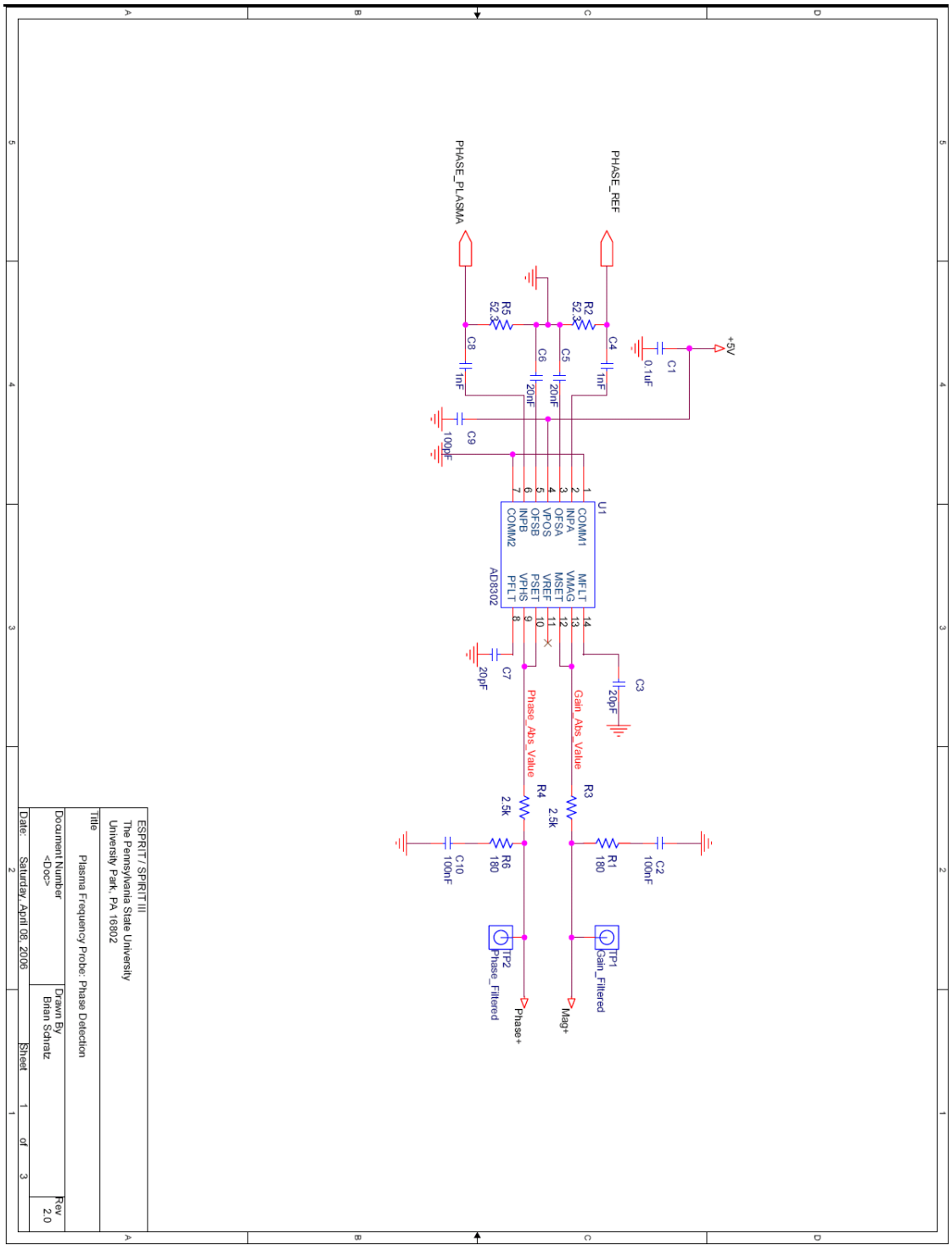

Figure **A-4**: Analog Board: Gain and Phase Detection

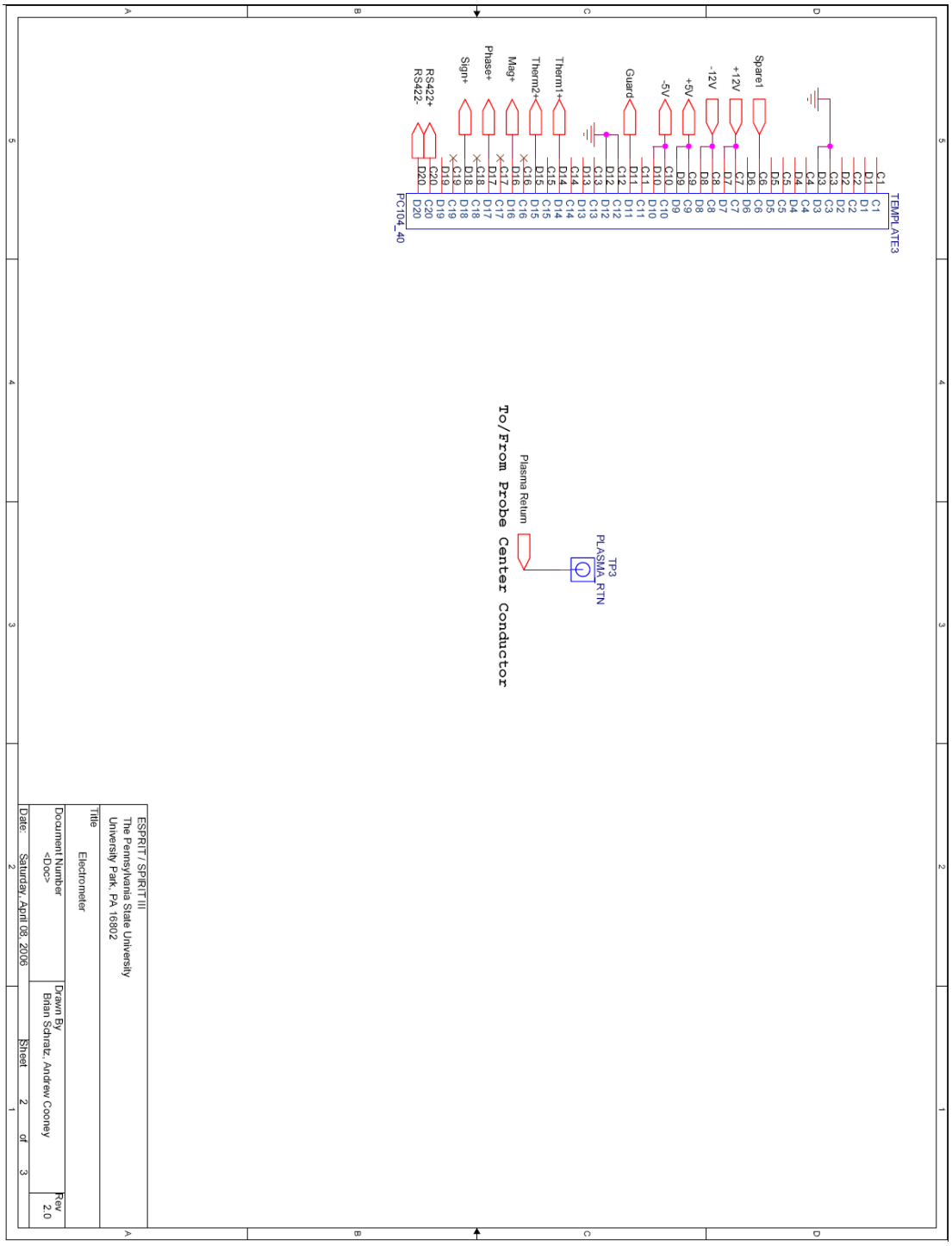

Figure **A-5**: Analog Board: Connectors

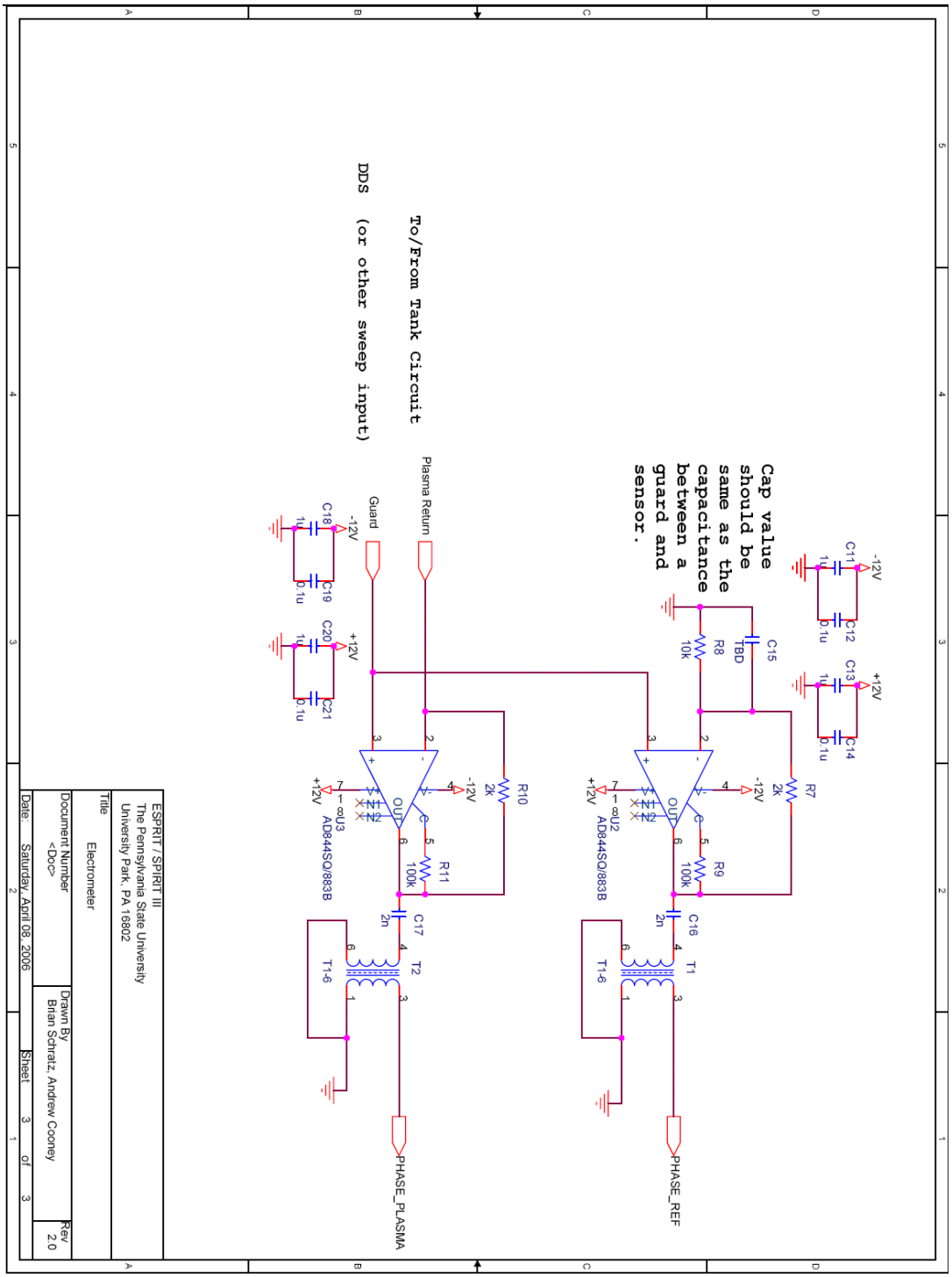

Figure **A-6**: Analog Board: Electrometer

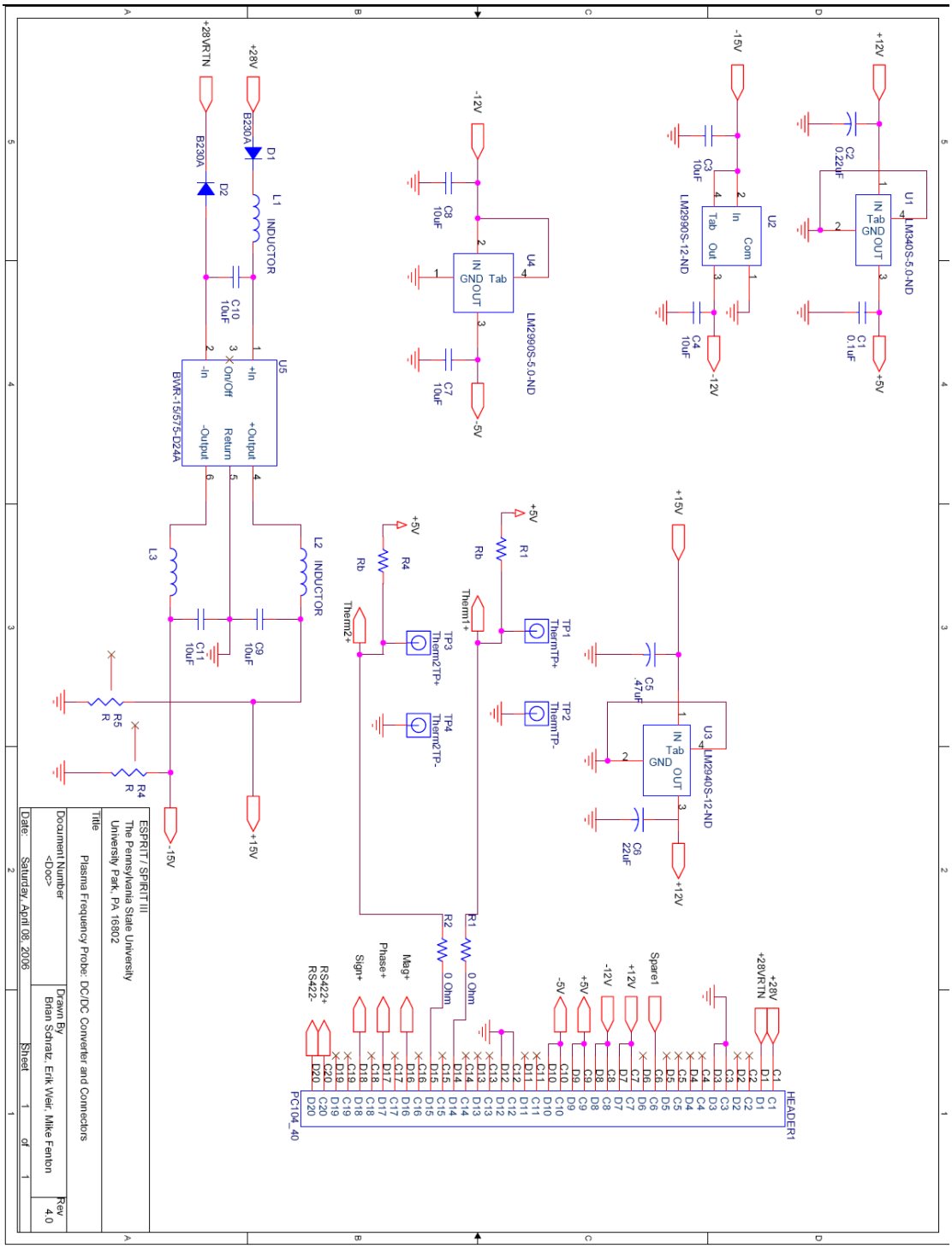

Figure **A-7**: Power Board

Appendix B

Microcontroller Code

```
; ###################################################################
;     Processor : MC9S12C32CFU16
;     FileFormat: V1.052
;     DataSheet : 9S12C-FamilyDGV1/D V01.00
;     Compiler  : Metrowerks C compiler
;     Date      : 03.06.2005
;     Abstract  :
;         This writes data from a table to the SPI input of
;         an Analog Devices AD9834 DDS device
;
;         After each update to the DDS, the step number of that
;         update is sent to the asynchronous port
;
;         File based on documentation found in the M68HC12B Family
;         datasheet (M68HC12B/D Rev. 8 7/2003, pages 204-226)
;         published by Motorola
;
;     Written by Brian Schratz
; ###################################################################

; export symbols
            XDEF Entry        ; export 'Entry' symbol
            ABSENTRY Entry    ; for absolute assembly: mark this as .
                              ;   application entry point

RAMStart  EQU  $0800  ; absolute address of RAM
ROMStart  EQU  $4000  ; absolute address to place code/constant data

; Register Equates
PTT         equ $0240  ; signals to AD7490       PORTOUT
DDRT        equ $0242  ; bit 0 as sclk
PORTAD0     equ $008F
ATTDDIEN    equ $008D

;****  Serial Peripheral Interface (SPI) Registers       *********
SP0CR1      equ $D8     ;SPI 0 Control Register 1
SP0CR2      equ $D9     ;SPI 0 Control Register 2
SP0BR       equ $DA     ;SPI 0 Baud Rate Register
SP0SR       equ $DB     ;SPI 0 Status Register
SP0DR       equ $DD     ;SPI 0 Data Register
SPISR       equ $DB
SPIDR       equ $DD

;****  Serial Communication Interface (SCI) Registers    *********
SCIBDH      equ $00C8
SCIBDL      equ $00C9
SCICR1      equ $00CA
SCICR2      equ $00CB
SCISR1      equ $00CC
SCISR2      equ $00CD
SCIDRH      equ $00CE
```

```
SCIDRL     equ $00CF

      ORG RAMStart
step  RMB 1

; ---------------------------------------------------------------------
; MAIN PROGRAM
; ---------------------------------------------------------------------

        ORG  ROMStart           ; 16K On-Board RAM, User code data area,
;                               ; start main program at $4000
Entry:
        LDS  #$900
        BSR  INIT            ; Subroutine to initialize SPI registers
MAIN:

; ---------------------------------------------------------------------
;* SWEEP
; ---------------------------------------------------------------------

NEWSWEEP
        ; Set the frequency pointer to zero
        LDY  #$0

        ; Set the step counter to zero
        MOVB #$0, step

LOOP1   ; Send LSB and increment the pointer to next byte
        LDD  FREQTABLE,Y
        BSR  SENDSPI
        INY
        INY

        ; Send MSB and increment the pointer to next byte
        LDD  FREQTABLE,Y
        BSR  SENDSPI
        INY
        INY

        JSR  Delay1sec

        ; Send the current frequency step to Telemetry
        BSR  SENDSCI

        ; Increment the step counter
        INC  step

        ; Is the end of the table reached?
        LDD  FREQTABLE,Y
        CPD  #$8888  ; Terminating Character
        BEQ  NEWSWEEP       ; Start sweep again if end is reached


        ; Continue the sweep
        BRA  LOOP1

; ---------------------------------------------------------------------
;* SUBROUTINE SENDSPI: No registers modified
; ---------------------------------------------------------------------
SENDSPI:
```

```
        PSHD
        PSHX

        MOVB #$FF, PTT

        JSR  DelayFF

        MOVB #$00, PTT

        BRCLR SPISR, #$20, *
        STAA SPIDR

        BRCLR SPISR, #$20, *
        STAB SPIDR

        BRCLR SPISR, #$20, *

        LDX  #$FFF
DelayFFF
        DEX
        BNE DelayFFF

        MOVB #$FF, PTT

        BSR DelayFF

        PULX
        PULD

        RTS

; ---------------------------------------------------------------------
;* SUBROUTINE SENDSCI: No Registers Modified
; ---------------------------------------------------------------------
        ; Transmits the value stored in Accumulator A using SCI

SENDSCI

        PSHA
        PSHY

        ; Clear SCI Status Register to begin communication
        SAME:     BRCLR SCISR1,#$80,SAME

        ; write data to serial data register
        LDAA step
        STAA SCIDRL

        ; Delay for testing
        LDY  #$FF
DELAY   DEY
        BNE DELAY

        PULY
        PULA

        RTS

; ---------------------------------------------------------------------
;* SUBROUTINE INIT: No registers modified
; ---------------------------------------------------------------------
```

```
INIT:
        PSHY
        PSHD

        ; Initialize SPI Registers for DDS
        MOVB #$FF, DDRT            ; Set Port T as output
        MOVB #$FF, ATTDDIEN        ; Set for Digital outputs on AD0

        MOVB #%01011010, SP0CR1
        MOVB #%00010000, SP0CR2
        MOVB #%00001111, SP0BR

        ; Initialize SCI Registers for Telemetry
        MOVB #$34, SCIBDL
        MOVB #$00, SCIBDH

        LDAA #$00
        STAA SCICR1; 8 bits no parity

        LDAA #$08
        STAA SCICR2; disabled, all serial int.

        ; Initialize DDS
        LDY  #$0

LOOP    LDD  INITTABLE,Y
        BSR  SENDSPI
        INY
        INY

        CPY  #$10
        BEQ  END_INIT

        BRA  LOOP

END_INIT
        PULD
        PULY

        RTS

; ---------------------------------------------------------------------
;* SUBROUTINE Delay1sec: No registers modified
; ---------------------------------------------------------------------
Delay1sec

        PSHA
        PSHX

        LDAA #$1
BIGLOOP

        LDX  #$FFFF
DELAYFFFF
        DEX
        BNE  DELAYFFFF

        DECA
        BNE  BIGLOOP

        PULA
```

```
        PULX

        RTS

; ---------------------------------------------------------------------
;* SUBROUTINE DelayFF: No registers modified
; ---------------------------------------------------------------------
DelayFF
        PSHX

        LDX  #$FF
DelayFF_loop
        DEX
        BNE  DelayFF_loop

        PULX

        RTS

; ---------------------------------------------------------------------
; TABLE
; ---------------------------------------------------------------------

        ORG $C100

INITTABLE
        FDB $2100    ; Control, load complete word in two writes, reset
        FDB $75C3    ; Freq0 lsb:
        FDB $40A3    ; Freq0 msb: = 500kHz
        FDB $B333    ; Freq1 lsb:
        FDB $8CCC    ; Freq1 msb: = 10MHz
        FDB $C000    ; Phas0 msb: 0000 0000 0000 = 0
        FDB $E000    ; Phas1 msb:
        FDB $2000    ; Control, load complete word in two writes, set
              ;01 FREQ0

FREQTABLE
        FDB $75C3 | FDB $7C48 | FDB $60A6 | FDB $763A
        FDB $40A3 | FDB $40B7 | FDB $40CE | FDB $40E7

        FDB $4E8D | FDB $67D2 | FDB $613B | FDB $4E71
        FDB $40A6 | FDB $40BA | FDB $40D1 | FDB $40EB

        FDB $6992 | FDB $55DB | FDB $649F | FDB $69CE
        FDB $40A8 | FDB $40BD | FDB $40D4 | FDB $40EE

        FDB $46D9 | FDB $466E | FDB $6ADC | FDB $485D
        FDB $40AB | FDB $40C0 | FDB $40D7 | FDB $40F2

        FDB $666A | FDB $7993 | FDB $73FC | FDB $6A2B
        FDB $40AD | FDB $40C2 | FDB $40DA | FDB $40F5

        FDB $484F | FDB $6F55 | FDB $400B | FDB $4F42
        FDB $40B0 | FDB $40C5 | FDB $40DE | FDB $40F9

        FDB $6C90 | FDB $67BD | FDB $4F13 | FDB $77B1
        FDB $40B2 | FDB $40C8 | FDB $40E1 | FDB $40FC

        FDB $5335 | FDB $62D4 | FDB $611F | FDB $6382
        FDB $40B5 | FDB $40CB | FDB $40E4 | FDB $4100
```

```
FDB $52C3
FDB $4104
FDB $4581
FDB $4108
FDB $7BC8
FDB $410B
FDB $75A5
FDB $410F
FDB $7327
FDB $4113
FDB $745B
FDB $4117
FDB $794E
FDB $411B
FDB $420E
FDB $4120
FDB $4EAA
FDB $4124
FDB $5F2F
FDB $4128
FDB $73AE
FDB $412C
FDB $4C34
FDB $4131
FDB $68D0
FDB $4135
FDB $4992
FDB $413A
FDB $6E89
FDB $413E
FDB $57C5
FDB $4143
FDB $4555
FDB $4148
FDB $774B
FDB $414C
FDB $6DB6
FDB $4151
FDB $68A7
FDB $4156
FDB $682E
```

```
FDB $415B
FDB $6C5E
FDB $4160
FDB $7547
FDB $4165
FDB $42FA
FDB $416B
FDB $558B
FDB $4170
FDB $6D0A
FDB $4175
FDB $498B
FDB $417B
FDB $6B20
FDB $4180
FDB $51DC
FDB $4186
FDB $7DD2
FDB $418B
FDB $6F15
FDB $4191
FDB $65BA
FDB $4197
FDB $61D5
FDB $419D
FDB $637A
FDB $41A3
FDB $6ABD
FDB $41A9
FDB $77B3
FDB $41AF
FDB $4A72
FDB $41B6
FDB $6310
FDB $41BC
FDB $41A2
FDB $41C3
FDB $663E
FDB $41C9
FDB $50FC
FDB $41D0
```

```
FDB $41F1
FDB $41D7
FDB $7935
FDB $41DD
FDB $76E0
FDB $41E4
FDB $7B09
FDB $41EB
FDB $45C9
FDB $41F3
FDB $5739
FDB $41FA
FDB $6F70
FDB $4201
FDB $4E89
FDB $4209
FDB $749D
FDB $4210
FDB $61C6
FDB $4218
FDB $561F
FDB $4220
FDB $51C3
FDB $4228
FDB $54CB
FDB $4230
FDB $5F56
FDB $4238
FDB $717D
FDB $4240
FDB $4B5E
FDB $4249
FDB $6D15
FDB $4251
FDB $56C0
FDB $425A
FDB $487D
FDB $4263
FDB $4269
FDB $426C
```

```
FDB $44A2
FDB $4275
FDB $4F49
FDB $427E
FDB $627C
FDB $4287
FDB $7E5C
FDB $4290
FDB $6307
FDB $429A
FDB $50A1
FDB $42A4
FDB $4749
FDB $42AE
FDB $4722
FDB $42B8
FDB $504D
FDB $42C2
FDB $62EE
FDB $42CC
FDB $7F28
FDB $42D6
FDB $651E
FDB $42E1
FDB $54F6
FDB $42EC
FDB $4ED3
FDB $42F7
FDB $52DB
FDB $4302
FDB $6135
FDB $430D
FDB $7A06
FDB $4318
FDB $5D76
FDB $4324
FDB $4BAD
FDB $4330
FDB $44D1
FDB $433C
FDB $490D
```

```
FDB $4348
FDB $588A
FDB $4354
FDB $7371
FDB $4360
FDB $59EE
FDB $436D
FDB $4C2B
FDB $437A
FDB $4A54
FDB $4387
FDB $5495
FDB $4394
FDB $6B1D
FDB $43A1
FDB $4E18
FDB $43AF
FDB $7DB6
FDB $43BC
FDB $7A24
FDB $43CA
FDB $4394
FDB $43D9
FDB $5A35
FDB $43E7
FDB $7E39
FDB $43F5
FDB $6FD1
FDB $4404
FDB $6F31
FDB $4413
FDB $7C8B
FDB $4422
FDB $5815
FDB $4432
FDB $4202
FDB $4442
FDB $7A88
FDB $4451
FDB $41DF
FDB $4462
FDB $583C
FDB $4472
FDB $7DD9
FDB $4482
FDB $72EE
FDB $4493
FDB $77B5
FDB $44A4
FDB $4C68
FDB $44B6
FDB $7143
FDB $44C7
FDB $6682
FDB $44D9
FDB $6C62
FDB $44EB
FDB $4321
FDB $44FE
FDB $6AFE
FDB $4510
FDB $6439
FDB $4523
FDB $6F13
FDB $4536
FDB $4BCE
FDB $454A
FDB $7AAB
FDB $455D
FDB $7BF0
FDB $4571
FDB $4FE0
FDB $4586
FDB $76C1
FDB $459A
FDB $70D9
FDB $45AF
FDB $7E72
FDB $45C4
FDB $5FD2
FDB $45DA
FDB $5544
FDB $45F0
FDB $5F14
FDB $4606
FDB $7D8C
FDB $461C
FDB $70FA
FDB $4633
FDB $79AB
FDB $464A
FDB $57F1
FDB $4662
FDB $4C1A
FDB $467A
FDB $5679
FDB $4692
FDB $7760
FDB $46AA
FDB $6F23
FDB $46C3
FDB $7E18
FDB $46DC
FDB $6496
FDB $46F6
FDB $62F3
FDB $4710
FDB $798A
FDB $472A
FDB $68B3
FDB $4745
FDB $70CC
FDB $4760
FDB $5231
FDB $477C
FDB $4D41
FDB $4798
FDB $625B
FDB $47B4
FDB $51E0
FDB $47D1
FDB $5C33
FDB $47EE
FDB $41B7
FDB $480C
FDB $42D4
FDB $482A
FDB $5FEE
FDB $4848
FDB $596F
FDB $4867
FDB $6FC1
FDB $4886
FDB $634E
FDB $48A6
FDB $7485
FDB $48C6
FDB $63D4
FDB $48E7
FDB $71AB
FDB $4908
FDB $5E7B
FDB $492A
FDB $6ABA
FDB $494C
FDB $56DA
FDB $496F
FDB $6355
FDB $4992
FDB $50A2
FDB $49B6
FDB $5F3B
FDB $49DA
FDB $4F9E
FDB $49FF
FDB $6248
FDB $4A24
FDB $57B8
FDB $4A4A
FDB $7071
FDB $4A70
FDB $6CF7
FDB $4A97
```

```
                FDB $7BAB       FDB $5096
        FDB $4DCE               FDB $4D59                               FDB $45FD
        FDB $4ABF                                       FDB $45D4       FDB $54E8
                                FDB $6F1E               FDB $50D4
        FDB $537E               FDB $4D8B                               FDB $452A
        FDB $4AE7                                       FDB $7767       FDB $5536
                                FDB $5102               FDB $5112
        FDB $7E91               FDB $4DBE                               FDB $4D12
        FDB $4B0F                                       FDB $6386       FDB $5585
                                FDB $6205               FDB $5152
        FDB $4F92               FDB $4DF1                               FDB $5EC4
        FDB $4B39                                       FDB $4B09       FDB $55D5
                                FDB $62D7               FDB $5193
        FDB $470F               FDB $4E25                               FDB $7B52
        FDB $4B63                                       FDB $6ECF       FDB $5626
                                FDB $542B               FDB $51D4
        FDB $6597               FDB $4E5A                               FDB $63D5
        FDB $4B8D                                       FDB $4FB8       FDB $5679
                                FDB $76B5               FDB $5217
        FDB $6BBC               FDB $4E8F                               FDB $5967
        FDB $4BB8                                       FDB $6EA9       FDB $56CD
                                FDB $4B2D               FDB $525A
        FDB $5A11               FDB $4EC6                               FDB $5D28
        FDB $4BE4                                       FDB $4C88       FDB $5722
                                FDB $524E               FDB $529F
        FDB $712D               FDB $4EFD                               FDB $703C
        FDB $4C10                                       FDB $6A41       FDB $5778
                                FDB $4CD3               FDB $52E4
        FDB $71A8               FDB $4F35                               FDB $53CB
        FDB $4C3D                                       FDB $48C2       FDB $57D0
                                FDB $7B7D               FDB $532B
        FDB $5C1B               FDB $4F6D                               FDB $4900
        FDB $4C6B                                       FDB $68FC       FDB $5829
                                FDB $5F0E               FDB $5372
        FDB $7124               FDB $4FA7                               FDB $510C
        FDB $4C99                                       FDB $4BE4       FDB $5883
                                FDB $784C               FDB $53BB
        FDB $7162               FDB $4FE1                               FDB $6D25
        FDB $4CC8                                       FDB $7274       FDB $58DE
                                FDB $47FF               FDB $5404
        FDB $5D75               FDB $501D                               FDB $5E84
        FDB $4CF8                                       FDB $5DA7       FDB $593B
                                FDB $4EF2               FDB $544F
        FDB $7601               FDB $5059                               FDB $6666
        FDB $4D28                                       FDB $4E7E       FDB $5999
                                FDB $4DF3               FDB $549B

        FDB $8888     ;DUMMY1
        FDB $8888     ;DUMMY1


;***************************************************************
;*                 Interrupt Vectors                           *
;***************************************************************
       ORG $FFFE

       fdb     Entry           ; Reset
```

Appendix C

Frequency Table Generation Matlab Script

```
% ************************************************************************
% *  Frequency Table Generator for Matlab 7.04                           *
% *  Plasma Frequency Probe                                              *
% *  SPIRIT III Sounding Rocket Project                                  *
% *  The Pennsylvania State University                                   *
% *  Written by:  Brian Schratz                                          *
% *  3 April 2006                                                        *
% ************************************************************************

% This program is designed to create a frequency table for the input data
% for the Analog Devices AD9834 Direct Digital Synthesizer.

% The user sets the start and stop frequencies and number of total
% steps in the following lines

% The program outputs a list for the LSB and MSB words for each frequency
% in the form [LSB MSB].  The table generates the values to update the
% FREQ0 register only.  Consult the AD9834 data sheet for details on
% writing to other registers and initialization.

% ************************************************************************
% User Modifiable Values:
%   Enter frequency in Hertz
     fstart = 100e3;
     fstop  = 10e6;

%   Enter number of steps in sweep
     numFreqs = 256;

% ************************************************************************

% All fixed values hereafter
f=logspace(log10(fstart),log10(fstop),numFreqs)';

% Calculate the values for the DDS input
    Fadjust=((2^28)*f)/(50000000); %see AD9834 Datasheet for this equation
    FadjustFloor=round(Fadjust); %round the values to the nearest integer

% Create the MSB
    % LOGICAL AND and shift out the MSB from the total word (14 data bits)
    MSB = bitand(FadjustFloor,268419072);
                        % 268,419,072 = 1111 1111 1111 1100 0000 0000 0000
    MSB = bitshift(MSB,-14);

    % Append 01 to identify the FREQ0 register and make the word 16 bits
    MSB = bitor(MSB,16384);  % 16384 = 0100 0000 0000 0000
    % Convert to hex
    MSB = dec2hex(MSB,4);

%Create the LSB
    % LOGICAL AND out the LSB from the total word (14 data bits)
```

```
    LSB = bitand(FadjustFloor,16383);     %     16383 = 11 1111 1111 1111
    % Append 01 to identify the FREQ0 register and make the word 16 bits
    LSB = bitor(LSB,16384);  % 16384 = 0100 0000 0000 0000
    % Convert to hex
    LSB = dec2hex(LSB,4);

% Output the two words together
[LSB MSB]
```

Appendix D

Mechanical Schematics

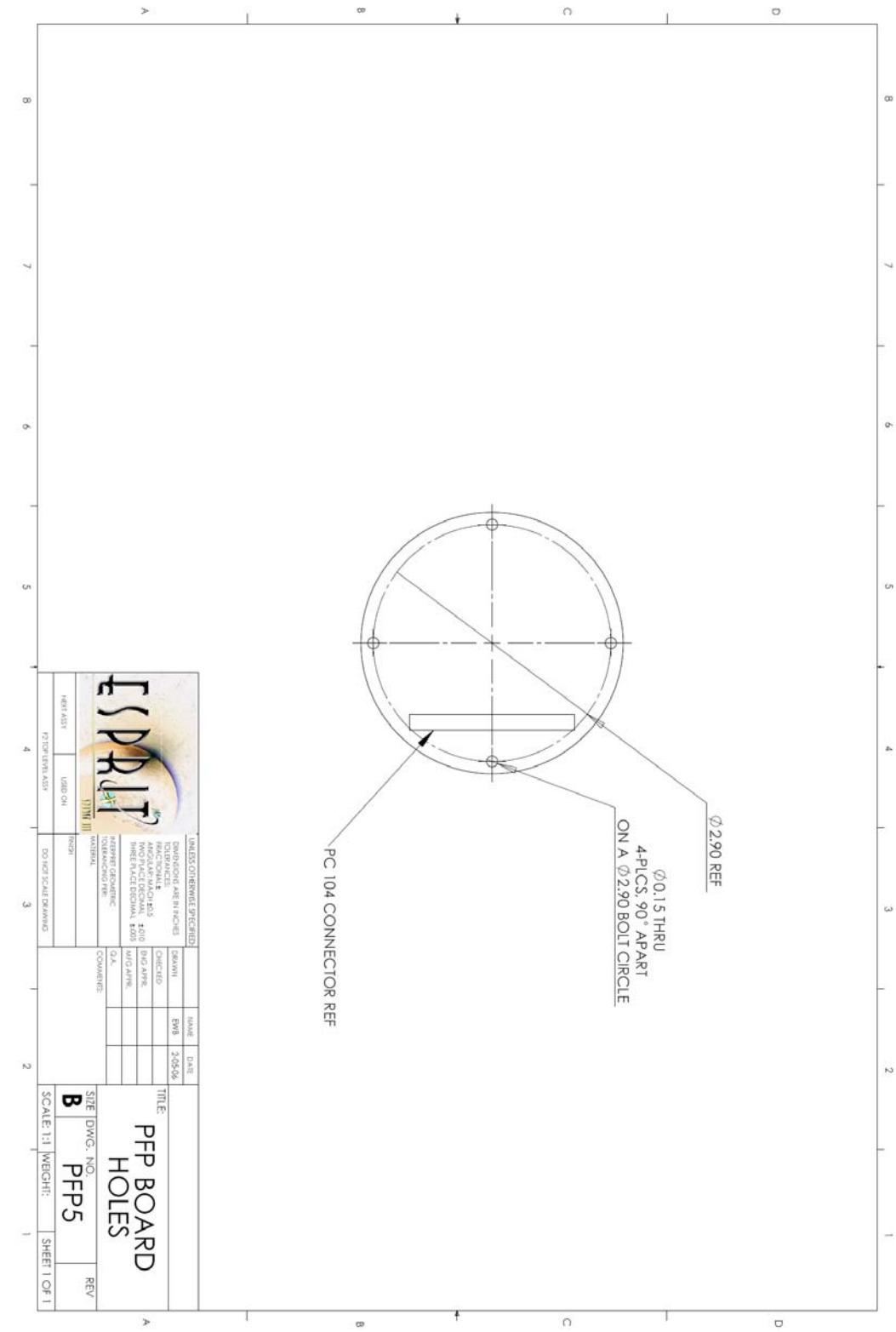

Figure **D-1**: PFP Board Holes

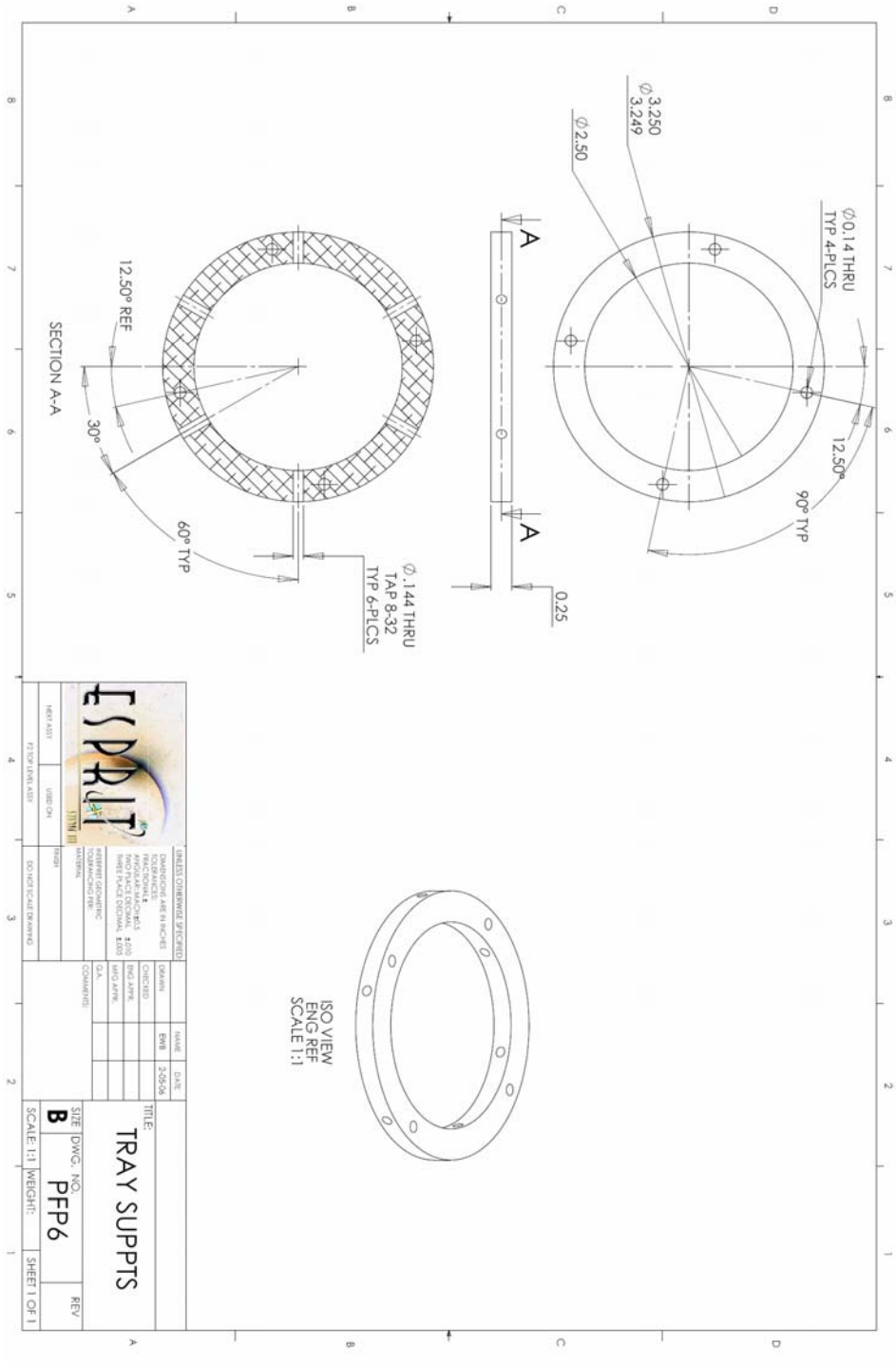

Figure **D-2**: Tray Support Ring

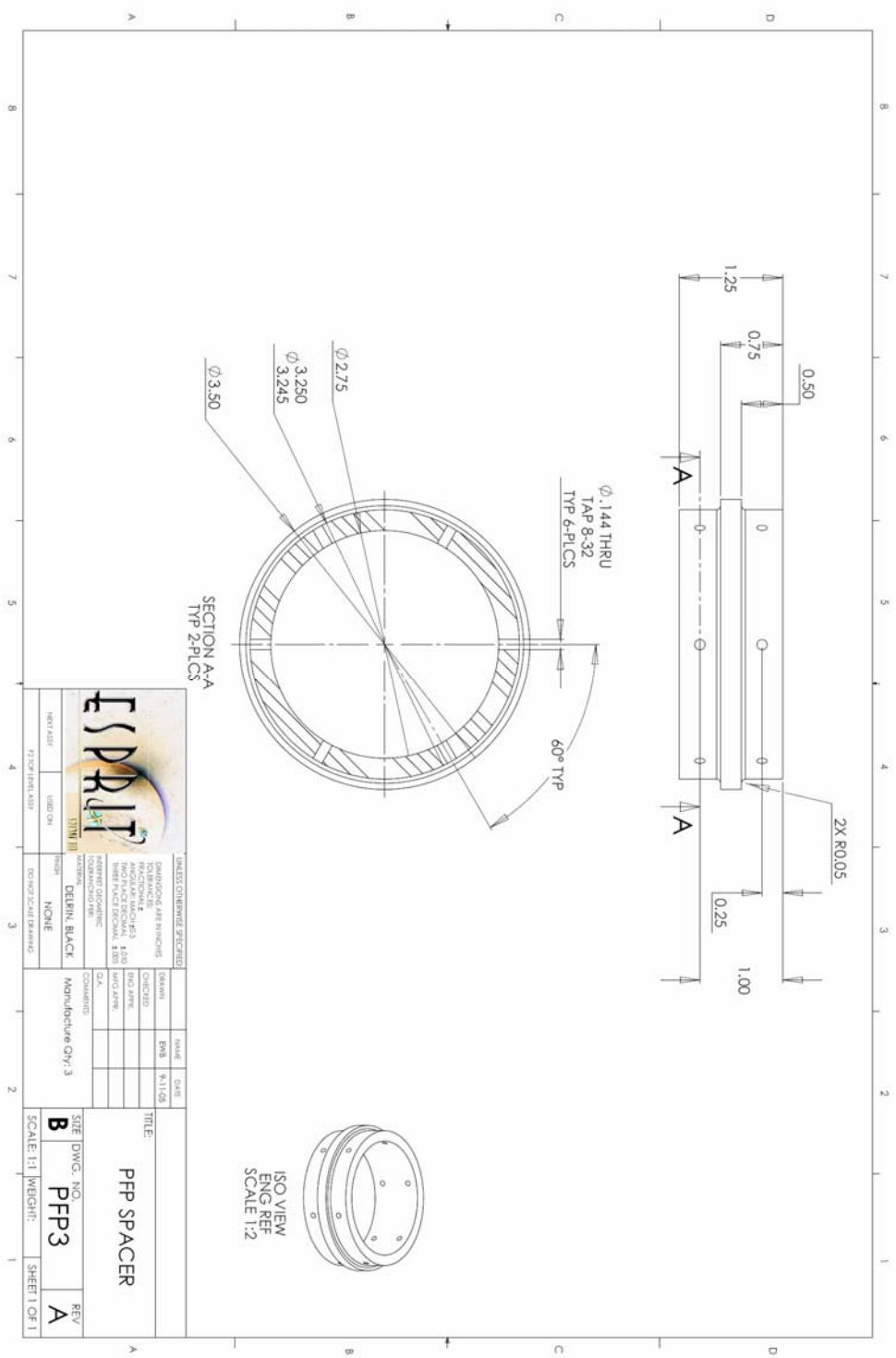

Figure **D-3**: Spacer

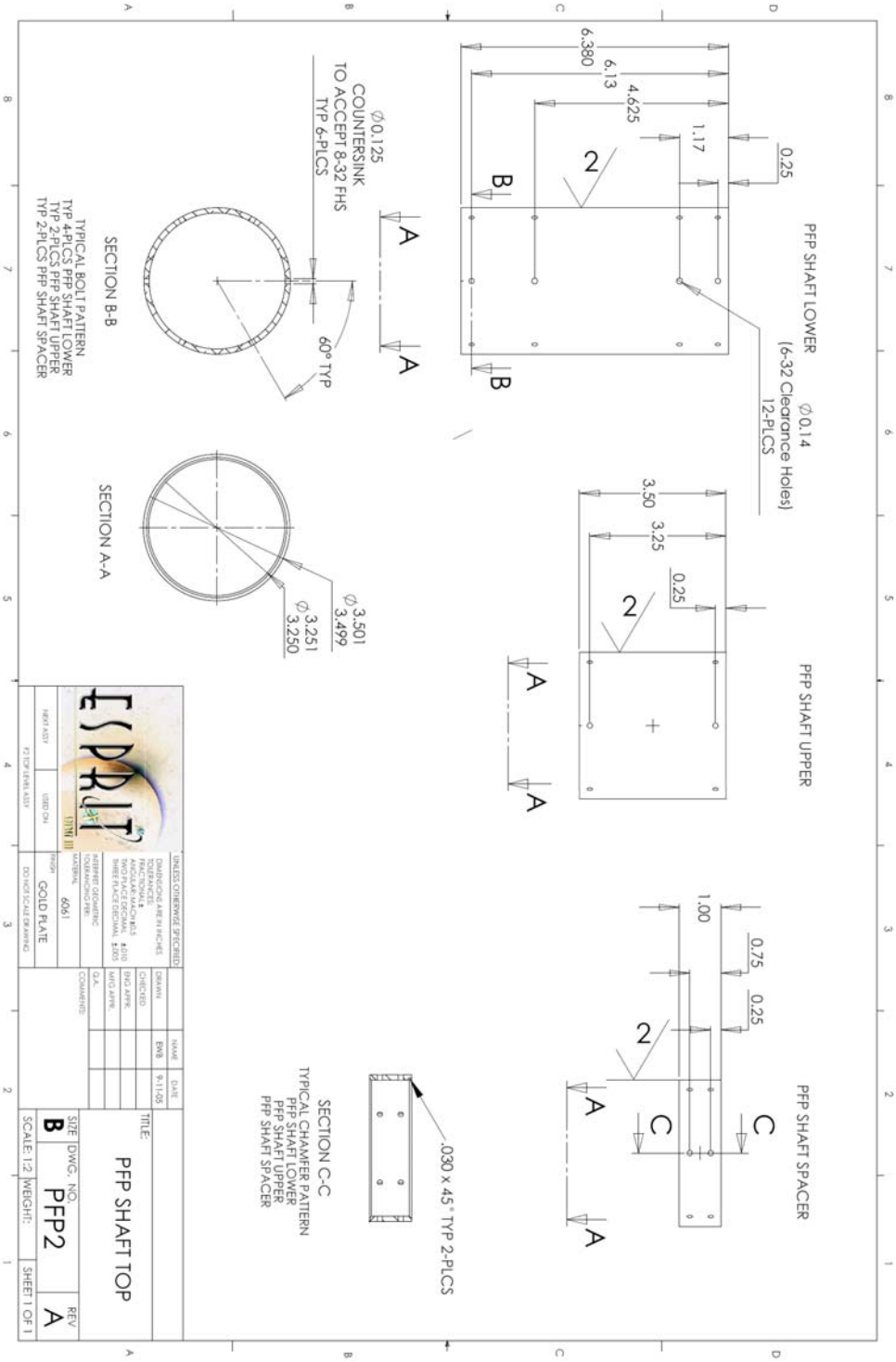

Figure **D-4**: Top Shaft

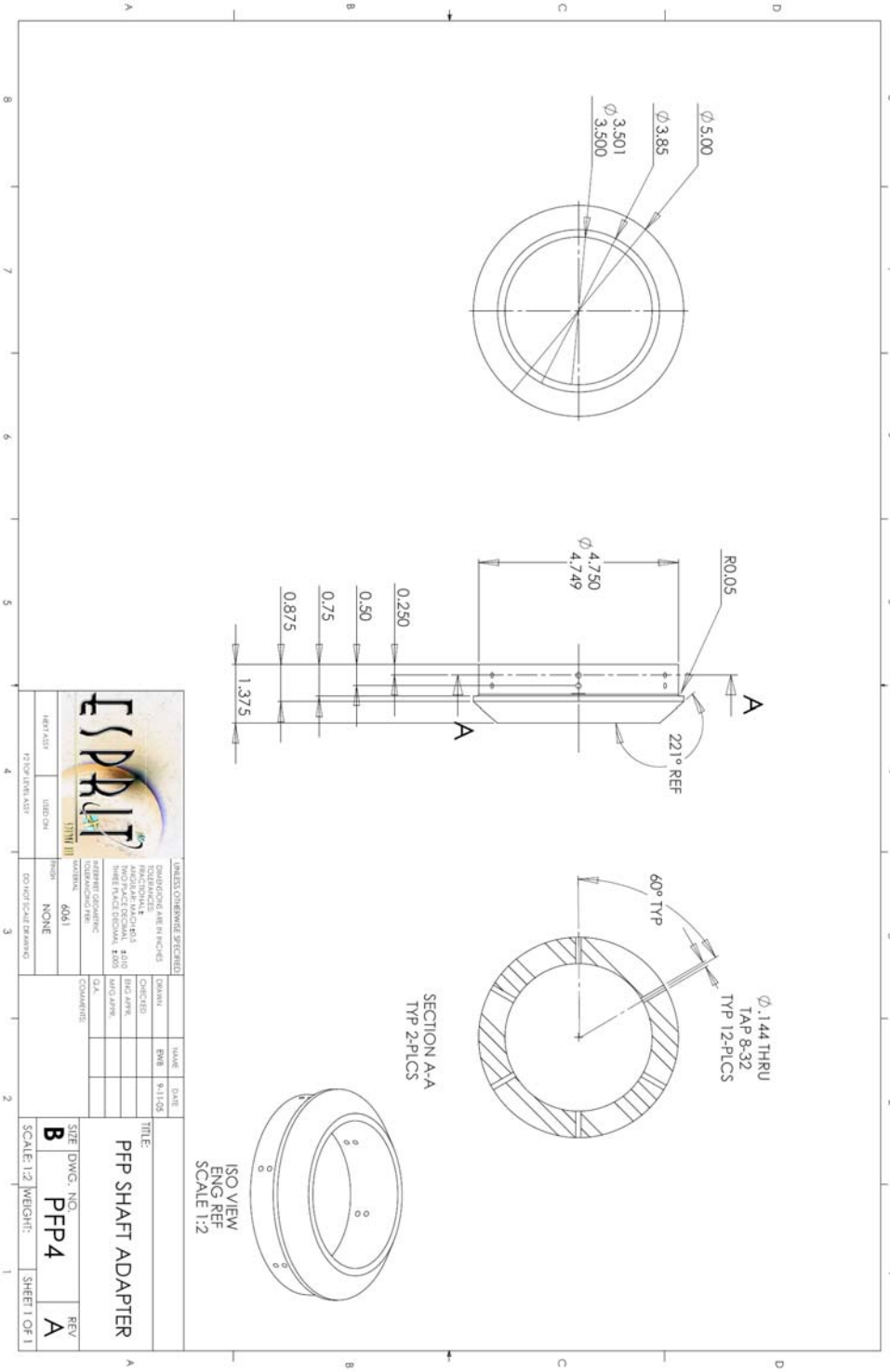

Figure **D-5**:Shaft Adapter

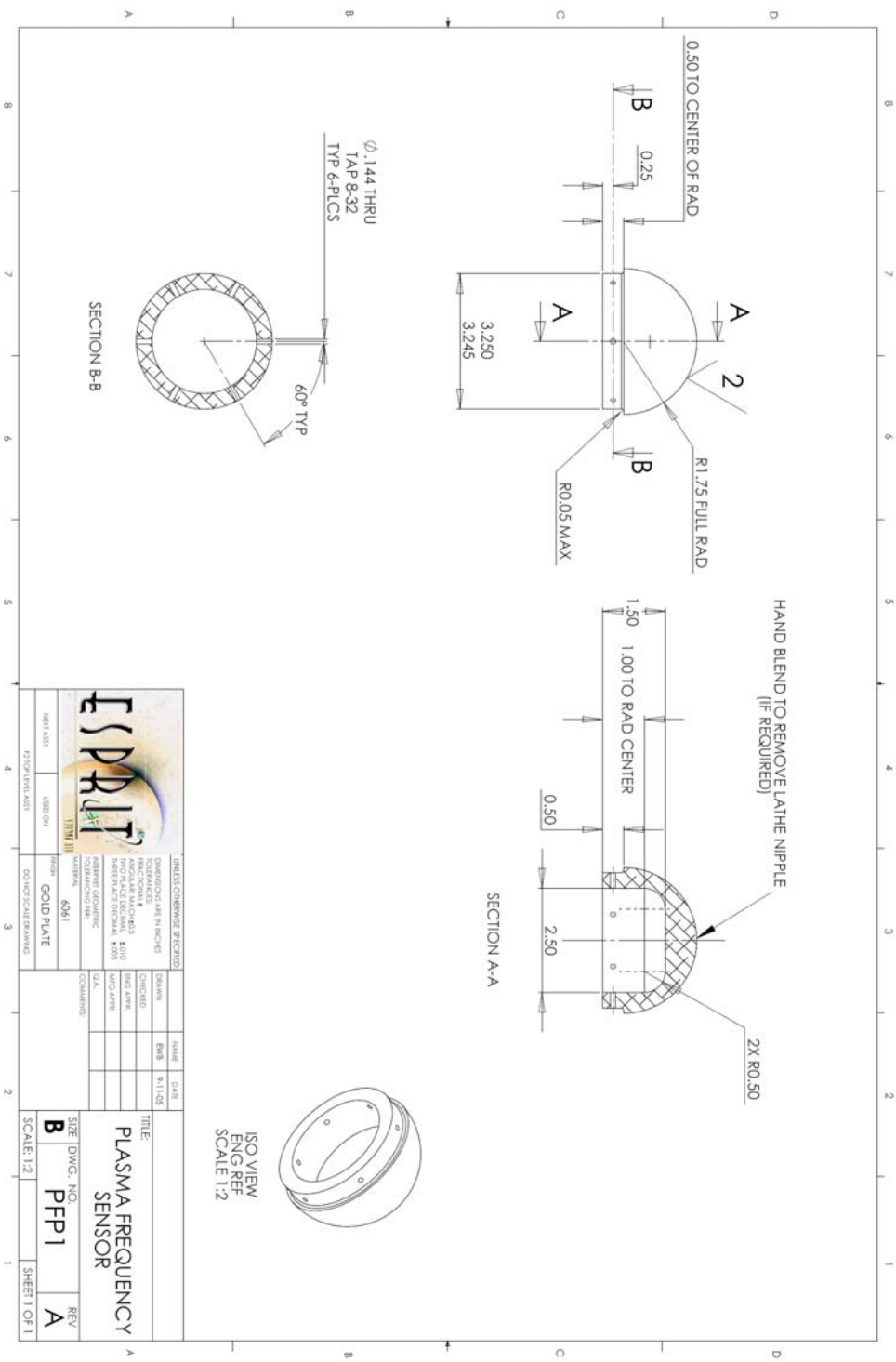

Figure **D-6**: Sensor Head

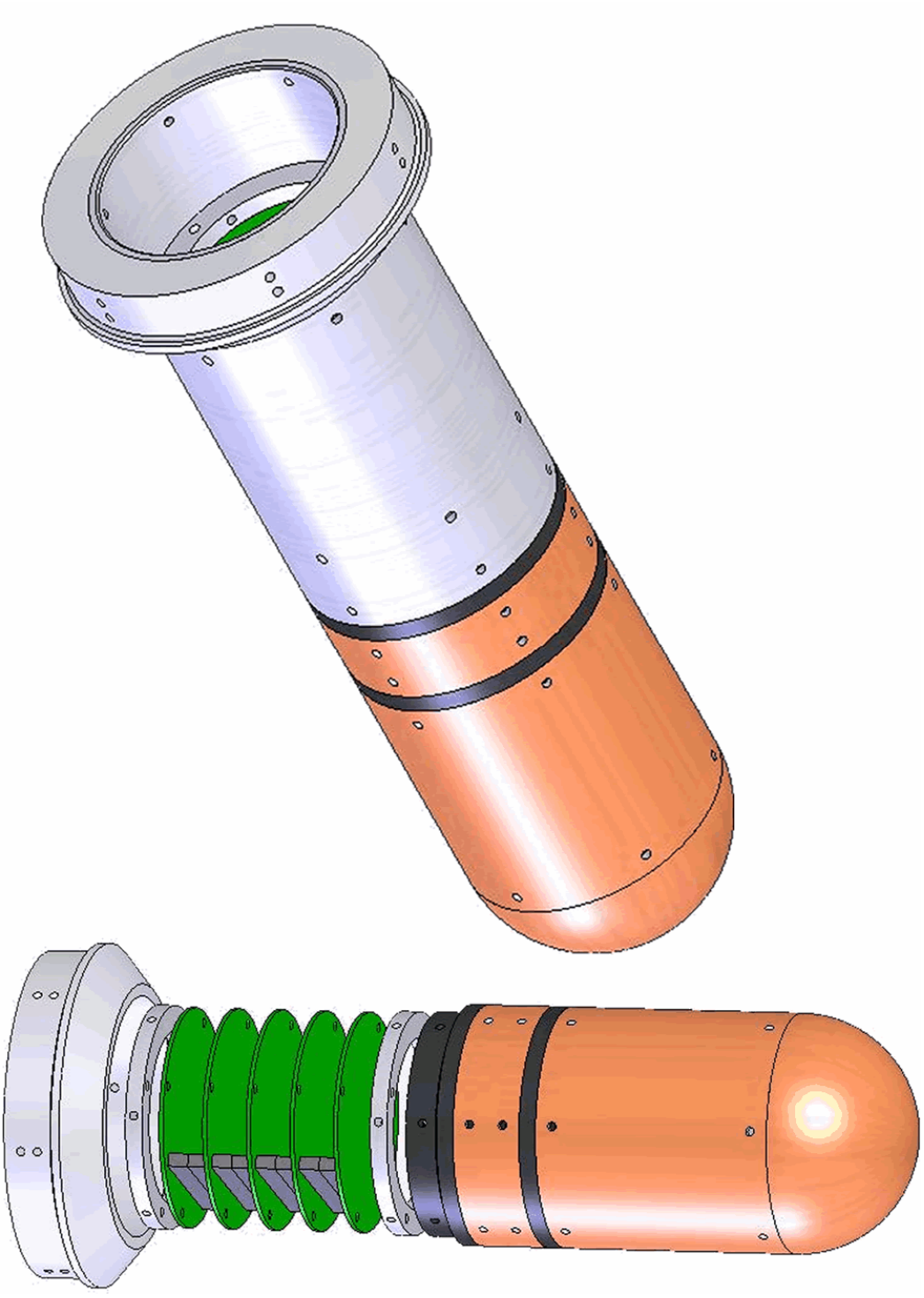

Figure **D-7**: Assembled instrument and arrangement of the internal electronics